Journal of Sedimentary Research
April 2025, Volume 95 Issue 2 Pages 223-238
https://doi.org/10.2110/jsr.2024.088
https://archimer.ifremer.fr/doc/00944/105553/

Geochemical and mineralogical characteristics of fjord sediments in Arctic Svalbard: insights into Holocene glacial activity and weathering variability

Jang Kwangchul [1, 2], Bayon Germain [3], Ahn Youngkyu [1], Joe Young Jin [1], Son Eun Jin [4], Kwon Sae Yun [4], Kim Jung-Hyun [1], Vogt Christoph [5], Forwick Matthias [6], Byun Eunji [2, *], Nam Seung-Il [1]

[1] Division of Glacier and Earth Sciences, Korea Polar Research Institute, 21990 Incheon, Republic of Korea
[2] Department of Earth System Sciences, Yonsei University, 03722 Seoul, Republic of Korea
[3] Université Brest, CNRS, Ifremer, Geo-Ocean, F-29280 Plouzané, France
[4] Division of Environmental Science and Engineering, Pohang University of Science and Technology, 37673 Pohang, Republic of Korea
[5] Crystallography and Geomaterials Research, FB05 Geosciences and MARUM, University of Bremen, Klagenfurter Strasse 2-4, 28359 Bremen, Germany
[6] Department of Geosciences, UiT The Arctic University of Norway, NO-9037 Tromsø, Norway

* Corresponding author : Eunji Byun, email address : eb@yonsei.ac.kr

Abstract :

The Svalbard archipelago at the border of the Arctic Ocean experiences substantial glacier retreat due to global warming, resulting in a retreat of glacier termini from the marine to terrestrial settings. However, the impact of these transitions on marine environments remains poorly understood. To improve our understanding of how Arctic Svalbard responds to fluctuations in climate and glaciers, we reconstructed past glacimarine environments in Hornsund, southern Svalbard, over the last 4,900 years. By tracking sediment provenance using detrital neodymium isotopes and quartz-to-carbonate ratios, we revealed a progression from nearly open-marine conditions with minimal glacial activity during the middle Holocene to gradual seaward glacial expansion into the Neoglacial period (4,000 years B.P. to 790 C.E.). Glaciers likely retreated landward during the Medieval Warm Period (MWP; 790 to 1,470 C.E.), punctuated by significant readvances at least twice. The Little Ice Age (LIA) witnessed multiple glacial advances into the marine environment, followed by an overall glacial retreat in modern times. Geochemical analysis of authigenic sediment components indicates pronounced enrichments of middle rare earth elements, particularly during rapid glacial advances such as the MWP and LIA, which we interpret as enhanced glacial erosion and accelerated sulfide oxidation. Paleo-analogues from the middle Holocene, characterized by minimal marine-terminating glaciers and reduced sulfide weathering, suggest potential future declines in sulfur-related bioessential nutrient fluxes into Arctic coastal environments and subsequently to marine ecosystems.

INTRODUCTION

Recent global warming has triggered unprecedented shifts in climate and environmental conditions (e.g., Diffenbaugh et al., 2017; Trenberth et al., 2014), particularly in the Svalbard archipelago – a rapidly warming region at the margin of the Arctic Ocean (Nordli et al., 2014). Rising temperatures have led to significant landscape changes in Svalbard, including negative glacier mass balance over approximately 30 years before 2,000 C.E. (Hagen et al., 2003) and a reduction in the glaciated area by up to 7% between pre-1,980 and 2,010 C.E. (Nuth et al., 2013). The recent acceleration of glacier mass loss (Kohler et al., 2007; Zemp et al., 2019) implies that many marine-terminating glaciers in Svalbard will turn into land-terminating glaciers in the near future. Among the most affected areas is the Hornsund Fjord in southern Svalbard, which has witnessed substantial glacial retreat over decades (e.g., Błaszczyk et al., 2019; Saferna et al., 2023) and even centuries (e.g., Pälli et al., 2003). Projections suggest that, if the current retreat trend of glaciers (e.g., Hornbreen and Hambergbreen) persists, the glaciated strait of eastern Hornsund may vanish in the near future (Grabiec et al., 2018), potentially isolating Sørkapp Land from the rest of Spitsbergen (Fig. 1). Given these drastic environmental changes, accurate forecasts of future environmental shifts in response to global warming are crucial for effective adaptation (e.g., Füssel, 2007). However, the accuracy of such predictions is hampered by limited environmental observations, which typically cover only a few hundred years. Past environmental reconstructions represent a crucial methodological approach, basing upon measured climate and environmental datasets to test the reliability of climate-model predictions (Braconnot et al., 2012; Lee et al., 2023).

Svalbard fjord sediments serve as an invaluable archive for reconstructing past glacial environments in response to climate fluctuations. Over the late Quaternary, Svalbard was covered by glaciers during cold intervals, but it also experienced major deglacial events during warm intervals (e.g., Hughes et al., 2016). Varying glacier extents have also been documented throughout the Holocene (Bartels et al., 2017; Forwick and Vorren, 2009; Hald et al., 2004; Salvigsen and Høgvard, 2006). For instance, glaciers reached their minimum extents during the early and/or middle Holocene (review in Farnsworth et al., 2020) and underwent substantial regrowth, referred to as the Neoglacial period, reaching their maximum postglacial extents (e.g., Werner, 1993). High-resolution sedimentary records for the Holocene thus offer valuable insights into the environmental response to various glacial states during periods dominated by either marine- or land-terminating glaciers or even in the nearly complete absence of glaciers. Since glacial activity has significant impact on land surface processes, such as physical abrasion and bedrock (or regolith) weathering (e.g., Anderson et al., 2000), Svalbard fjord sediments deposited during the Holocene can archive useful information about weathering processes and other environmental changes linked to past glacial dynamics. Such sedimentary records can provide glimpses of potential future environmental conditions resulting from global warming, hence emphasizing the importance of reconstructing high-resolution past environments in Svalbard.

In this study, we investigate glacimarine environmental changes in Hornsund over the last 4,900 years, based on neodymium (Nd) isotope and bulk mineralogical data from a sediment core. By identifying the Nd isotope signature and mineralogical properties of potential sediment sources, based on reported datasets for various surface sediments in Hornsund, we are able to trace changes in sediment provenance and corresponding glacier configuration. Additionally, we report abundances of rare earth elements (REEs) for Fe-(oxyhydr)oxide phases leached from bulk sediments, which provide particular insight into sulfide oxidation processes linked to glacial weathering. We show that sustained sulfide oxidation prevailed throughout the entire period, being most likely more intense at times of glacial advances.

STUDY AREA

The Svalbard archipelago is located at the border between the Arctic and the N. Atlantic Oceans, encompassing all islands situated between 74-81° N and 15-35° E, including Spitsbergen, Barentsøya, Edgeøya, and Nordaustlandet (Fig. 1). Over the late Quaternary period, this archipelago has undergone repeated glacier advances and retreats in response to climate variability. For example, during the last glacial maximum, Svalbard was almost entirely glaciated (Hughes et al., 2016), whereas currently, approximately 57% of its land area remains glaciated (Nuth et al., 2013).

Hornsund is the southernmost fjord in the western part of Spitsbergen. This fjord is approximately 32 km long in an east-west direction and up to 10 km wide. It comprises one main basin and five sub-basins, Brepollen, Samarinvågen, Austre and Vestre Burgerbukta, and Isbjörnhamna (Fig. 1), all affected by tidewater glaciers. The main basin is > 250 m deep, while water depths in the sub-basins range from 55 m in Isbjörnhamna to 180 m in Vestre Burgerbukta. The hydrography in Hornsund is governed primarily by the interplay between advected regional seawater and local glacial meltwater (Beszczynska-Moller et al., 1997). The warm Atlantic Water and the cold Arctic Water, transported by the West Spitsbergen Current and the East Spitsbergen Current, respectively, contribute to the oceanic water masses in the region (Fig. 1). Glacial meltwater runoff not only causes significant hydrological perturbation but also leads to rapid sediment accumulation (Błaszczyk et al., 2019; Görlich, 1986).

The bedrock geology around Hornsund exhibits significant diversity (Dallmann and Elvevold, 2015) (Fig. 1). The catchment areas of western Hornsund are characterized by Proterozoic metamorphic rocks, including phyllites, schists, quartzites and marbles, while those around the central fjord correspond to Cambrian to Ordovician carbonate rocks such as marbles, limestones, and dolostones. On the other hand, the bedrock geology surrounding eastern Hornsund is composed predominantly of upper Paleozoic to Lower Cretaceous sedimentary rocks. In the easternmost glacial catchment area, Paleogene sedimentary rocks also prevail.

Three main periods of glacier advance have been identified during the Holocene. The oldest, known as the Grönfjorden Stage, commenced before 8 kyr B.P. (Marks and Pekala, 1986). Subsequently, the Revdalen stage occurred around 3.0-2.5 kyr B.P. (Karczewski et al., 1981). After glacial retreat, a renewed glacier advance followed during the Little Ice Age (LIA), dated to 0.6-0.1 kyr B.P. (Lindner and Marks, 1993 and references therein). In Hornsund, the maximum glacier extent during the LIA reached near the western boundary of Brepollen and the southern boundary of Burgerbukta (Błaszczyk et al., 2013). In comparison, during the Revdalen stage, the glacier extended beyond the western boundaries of Isbjörnhamna to the north and Gåshamna to the south (Lindner and Marks, 1993; Lindner et al., 1984). It is noteworthy that the glacier expansion event in Hornsund has been reported to occur before the LIA between ~ 2.0 and 1.5 kyr B.P., based on ^{10}Be dating of moraines (Philipps et al., 2017).

MATERIALS AND METHODS

Sample Collection

The gravity core HH19-878-GC (76º57.543' N, 15º41.886' E, water depth 125 m, 405 cm long) was retrieved from the western parts of the central basin of Hornsund during the Korea-Norway joint expedition of *RV Helmer Hanssen* (UiT The Arctic University of Norway) in 2019 (Fig. 1). The wet bulk density and magnetic susceptibility of the whole core were measured in 1-cm intervals using a GEOTEK Multi-Sensor Core Logger at UiT. After splitting the core, a half-core section was used for acquiring x-radiographs and line-scan images using a GEOTEK Standard X-ray CT System and an Avaatech X-ray fluorescence core scanner, respectively, at UiT (cf. Joe et al., 2022). Another half-core section was subsampled at 1 cm intervals and then freeze-dried for additional analyses.

Grain-Size Distribution

The grain-size analysis was conducted at 5 cm intervals using a Malvern Mastersizer 3000 laser diffraction particle size analyzer at Korea Polar Research Institute (KOPRI). Before the analysis, ~ 130 mg of sediments were treated with 35% hydrogen peroxide for 24 hours to eliminate the organic matter, followed by thorough rinsing with deionized water (18.2 MΩ, Millipore). Mean grain sizes were calculated with GRADISTAT v 8.0 (Blott and Pye, 2001) based on the method of Folk and Ward (1957). Grains larger than 1 mm were counted at 5 cm intervals from x-radiographs. Additionally, the proportion of grains > 63 μm was determined at 10 cm intervals via manual wet sieving.

AMS ^{14}C Age Dating

We collected marine mollusc shells and mixed benthic foraminifers from sediments > 63 μm at these depths: 4-5, 54-55, 59-60, 79-80, 104-105, 114-115, 139-140, 149-150, 179-180, 214-215, 249-250, 309-310, 359-360, 389-390 and 399-400 cm (n = 15). These samples were analysed at the BETA Analytic Laboratory (Miami, USA) or the Alfred Wegener Institute (Bremen, Germany) for AMS ^{14}C dating (Table 1). All ^{14}C dates were used to establish the age-depth relationship at 0.5 cm intervals through Bayesian age-depth models, BACON v. 3.2.0 (Blaauw and Christen, 2011). In this model, ^{14}C dates were initially converted to calendar ages based on the Marine20 calibration curve (Heaton et al., 2020), applying a reservoir age offset of –61 ± 37 years in western Svalbard (Pieńkowski et al., 2022). The age of the core surface was established as 2019 C.E.. While we generally adhered to the default settings of BACON, we made a slight adjustment to the Student's t-distribution parameters, *t.a.* and *t.b.*, changing from 3 and 4 to 33 and 34, respectively. This modification aligns with previous studies conducted in Svalbard (Jang et al., 2021, 2023; Joe et al., 2022), resulting in a less smoothed age-depth relationship. The weighted mean age at each depth provided by BACON was used as the final age estimate in this study, along with the uncertainty at the 95% confidence level calculated based on Markov Chain Monte Carlo iterations.

Rare Earth Element Concentrations and Neodymium Isotopes

Rare earth element (REE) concentrations and neodymium isotope compositions were measured from two different components within sediments, defined as "authigenic" and "detrital" fractions, at every 5 to 50 cm intervals. The authigenic fraction primarily corresponds to hydrogenous Fe-(oxyhydr)oxides extracted from bulk sediments with a mixed solution of 0.02

M hydroxylamine hydrochloride in 25% acetic acid (v/v) buffered to pH of 4.5 (referred to as HH solution from herein) for 1 hour (Jang et al., 2021). To minimize the potential dissolution of reactive terrigenous materials during leaching, the reagent-to-sediment ratio was maintained at approximately 1 (Jang et al., 2017; Wilson et al., 2013). The remaining detrital fraction, conversely, comprised materials devoid of authigenic components. To remove any authigenic remnants from the sediments, an extra chemical leaching process was conducted using the HH solution, with a higher reagent-to-sediment ratio of approximately 10, for over 24 hours. Following this leaching process, the residual detrital fractions were fused with a mixture of sodium peroxide and sodium hydroxide in a furnace at ~ 650 °C for 15 minutes (Bayon et al., 2009).

The concentrations of REEs in the aliquots of both authigenic and detrital fractions were determined with a Thermo Scientific Element XR sector field Inductively Coupled Plasma Mass Spectrometer at the Pôle Spectrométrie Océan (Brest, France), using the Tm addition method (Barrat et al., 1996). Isobaric interferences were corrected using oxide formation rates determined via analysis of mono-elemental solutions (Ba-Ce, Nd-Pr, and Sm-Eu-Gd-Tb). The internal error for all measurements was consistently below 5%. The accuracy was evaluated by analysing various geological certified reference materials (AGV-1; AN-G; BCR-1; DR-N; UB-N; WS-E; and IF-G, i.e., an iron-ore deposit), which provided concentrations consistent with reference values (< 13%).

Before isotopic analyses, pure fractions of Nd were isolated with a two-stage column separation protocol using both TRU (50-100 μm, Eichrom) and Ln resins (50-100 μm, Eichrom), following a method adapted from Pin and Zalduegui (1997). The purified Nd fractions from both authigenic and detrital fractions were then loaded onto Re filaments for isotopic analysis using a thermal ionization mass spectrometer (TIMS, Triton, Thermo Scientific) at KOPRI. Mass fractionation during analysis was corrected by normalizing measured $^{143}Nd/^{144}Nd$ ratios to $^{144}Nd/^{146}Nd = 0.7219$. Long-term replicate analyses of the JNdi-1 standard yielded $^{143}Nd/^{144}Nd = 0.512121 \pm 0.000008$ (2 SD, n = 14), consistent with the reference value (Tanaka et al., 2000). The inferred external reproducibility is 0.2 ε_{Nd} units, ($\varepsilon_{Nd} = [(^{143}Nd/^{144}Nd)_{sample}/(^{143}Nd/^{144}Nd)_{CHUR}-1] \times 10^4$, $(^{143}Nd/^{144}Nd)_{CHUR} \sim 0.512638$ from Jacobsen and Wasserburg, 1980). The accuracy was assessed using certified reference materials (BCR-2, BHVO-2), yielding $^{143}Nd/^{144}Nd$ ratios consistent within uncertainty with the literature values (Weis et al., 2006). Duplicate analyses are also consistent with each other within analytical uncertainty.

TOC, $\delta^{13}C_{org}$, and N_{org}

The total organic carbon (TOC) contents and its isotopic ratios ($\delta^{13}C_{org}$) were determined using a Thermo Delta V Isotope Ratio Mass Spectrometer connected to a Thermo Flash 2000 Elemental Analyzer at KOPRI. Before the analysis, freeze-dried samples, collected at every 5 cm intervals, were powdered using an agate mortar and pestle. Subsequently, the samples were acidified with 2M hydrochloric acid for 24 hours to remove inorganic carbonate. The decarbonated samples were thoroughly rinsed with deionized water (18.2 MΩ, Millipore) and then freeze-dried for loading onto the analyzer. The reported $\delta^{13}C_{org}$ values are expressed in per mil notation relative to the Vienna Pee Dee Belemnite international standard. Duplicate analyses of TOC and $^{13}C_{org}$ show average standard deviations of less than 0.2% and 0.15‰, respectively.

Regarding organic nitrogen (N_{org}) content, bulk sediment samples, also collected at 5 cm intervals, were powdered and divided into two aliquots. The first aliquots were used to determine total nitrogen content, while the second aliquots were used to measure inorganic nitrogen content after the complete removal of organic nitrogen using a KOBr-KOH solution (Silva and Bremner, 1966). Contents of total and inorganic nitrogen were measured using the Thermo Flash 2000 Elemental Analyzer at KOPRI. The N_{org} content was then calculated by subtracting the inorganic-nitrogen content from the total-nitrogen content, with a reproducibility of less than 0.2%.

Bulk Mineral Assemblage

Mineralogical analysis of bulk powdered sediments at 5 cm intervals in core HH19-878-GC (n = 82) was performed using a Philips X'Pert Pro multipurpose diffractometer at the University of Bremen, Germany (for detailed setting, see Jang et al., 2023). The Philips software X'Pert HighScore™ was used primarily to identify the main mineral assemblages, while Apple MacIntosh X-ray diffraction interpretation software MacDiff 4.25 was used for sheet silicates (Petschick et al., 1996). Mineralogical quantification was carried out using the QUAX full-pattern method based on a reference material database (Vogt et al., 2002).

In this study, we focused exclusively on the abundance of quartz, calcite, dolomite, and Fe-(oxyhydr)oxides. The reported abundance of Fe-(oxyhydr)oxide in this study includes crystalline Fe-(oxyhydr)oxide, such as hematite, goethite, and lepidocrocite, but specifically excludes magnetite and amorphous Fe-(oxyhydr)oxides. Analytical uncertainties, determined through tests on artificial mixtures including the Reynolds Cup (Raven and Self, 2017), were found to be better than 1-3% for well-crystallized minerals like quartz and calcite, and 10% for Fe-(oxyhydr)oxide (Vogt et al., 2002). The full XRD results can be accessed at the Korea Polar Data Center (https://kpdc.kopri.re.kr/).

RESULTS

Sediment Lithology

Core HH19-878-GC consists primarily of brown-colored sandy mud (Fig. 2). Significant changes in sediment color and primary structures are absent. Bioturbation is prevalent throughout the entire core, with varying degrees and features. The wet bulk density fluctuates between 1.62 and 1.86 g/cc (average 1.73 ± 0.05, 1 SD, n = 398), while magnetic susceptibility varies from 8.14 to 16.0 × 10^{-5} (10.0 ± 0.78 × 10^{-5}, 1 SD, n = 376) (Fig. 2 and Supplementary Table S1). The grain-size distribution exhibits a general-coarsening trend downcore, with a mean grain size ranging from 7.0 to 16.5 μm (Fig. 2 and Supplementary Table S1). Notably, x-radiographs show intermittent occurrences of grains larger than 1 mm size, including pebbles and boulders (hereafter referred to as ice-rafted debris, IRD; compared with Forwick and Vorren, 2009), with their sizes and amounts displaying considerable variability (Fig. 2).

Chronology

Measured radiocarbon dates are listed in Table 1 and Figure 2. Age inversions occurred repeatedly at depths of 59-60, 79-80, 114-115, 139-140, 179-180, and 389-390 cm, regardless of material types used in the analysis. These anomalies are typically interpreted as sediment reworking (Flink et al., 2018). The age-depth relationship established by BACON indicates that core HH19-878-GC spans approximately 4.9 kyr (Fig. 3 and Supplementary Table S2). The average sedimentation rate is estimated at ~ 0.08 cm/yr, slightly lower than that of nearby core HF_2011 (76º57.238' N, 15º41.782' E, water depth 135 m from Pawłowska et al., 2016; for location, see Fig. 1).

Geochemical and Mineralogical Data

Nd isotopes.--- Detrital ε_{Nd} values in core HH19-878-GC do not show any significant correlation with the authigenic ε_{Nd} values (r = -0.13, n = 21) (Fig. 4 and Supplementary Table S3). The detrital ε_{Nd} values vary from -15.5 to -12.5 (-13.9 ± 0.9, 1 SD, n = 21), showing a saw-tooth pattern with short-lived ε_{Nd} excursions towards both unradiogenic and radiogenic values between approximately 500 C.E. and 1,600 C.E.

On the other hand, authigenic ε_{Nd} values vary within a narrower range from -10.6 to -9.6 (-10.2 ± 0.2, 1 SD, n = 21) (Fig. 4 and Supplementary Table S3). These ε_{Nd} values are slightly higher than the regional ε_{Nd} signature for seawater on the western Svalbard shelf (i.e. the Sørkapp Current, with ($-11.6 < \varepsilon_{Nd} < -10.6$ from Laukert et al., 2017), but they are comparable to or lower than the reported ε_{Nd} values of authigenic fractions in surface sediments collected from Brepollen, the innermost part of Hornsund ($-10.4 < \varepsilon_{Nd} < -9.0$ from Jang et al., 2020). Overall, no distinct temporal trend is observed in authigenic ε_{Nd} values, given the analytical uncertainty.

REE concentrations.--- The sedimentary REE abundances in core HH19-878-GC are expressed as concentrations (μg/g) relative to the initial mass of bulk sediments (Supplementary Table S4). Detrital sediments show REE concentrations approximately two orders of magnitude higher than those in authigenic sediments. For instance, lanthanum (La) concentrations in detrital sediments range from 19.7 to 54.5 μg/g, corresponding abundances in authigenic sediments vary from 0.37 to 0.66 μg/g. Likewise, gadolinium (Gd) and ytterbium (Yb) concentrations in detrital sediments fall within the ranges of 2.45-5.56 μg/g and 1.32-3.10 μg/g, respectively, while authigenic sediments exhibit much lower concentrations (0.25-0.42 μg/g for Gd and 0.05-0.09

μg/g for Yb). Notably, the REE abundances in detrital sediments at this site display flat patterns when normalized to world river average silt values (WRAS; Bayon et al., 2015) (Fig. 5). Conversely, the WRAS-normalized REE patterns in corresponding authigenic sediments show strong mid-REE enrichments relative to light- and heavy-REE (Fig. 5). The different degrees of mid-REE enrichments can be quantified using the "concavity index (CI)", calculated as $Gd_N/(La^6_N \times Yb^7_N)^{1/13}$ (Bayon et al., 2020), which results in calculated CI values of 0.9-1.0 and 3.0-4.6, for detrital and authigenic sediments, respectively.

Organic geochemistry (TOC, $\delta^{13}C_{org}$ and N_{org}).--- The average contents of TOC and N_{org} are 1.54 ± 0.08 wt.% (1 SD, n = 81) and 0.22 ± 0.08 wt.% (1 SD, n = 42), respectively (Fig. 6 and Supplementary Table S4). Both contents display general upward-decreasing trends although TOC contents display a somewhat scattered distribution. The combined ratios of TOC/N_{org} show wide fluctuations between 12 and 43. These ratios generally increase upward, reaching a maximum at 1,900 C.E., and then decrease back to 22. Conversely, $\delta^{13}C_{org}$ values generally decrease upward, although their variability is relatively narrower in the range between -25.0 and -23.6. Note the absence of pronounced peaks in the uppermost part of the core.

Mineralogical abundance.--- Calcite contents determined by XRD range from 2.5 to 11.3 wt.% (6.9 ± 2.5 wt.%, 1 SD, n = 82) (Fig. 6 and Supplementary Table S5), being generally higher in the lower part of the core and gradually decreasing upward. Dolomite contents fluctuate from 0 to 10.9 wt.%, with an average content of 3.0 ± 2.1 wt.% (1 SD, n = 82). This mineral is also more abundant in the lower part of the core than in the upper part. However, the upward decreasing trend of dolomite is less pronounced than calcite.

Quartz contents do not display any significant trend downcore. The average quartz content in core HH19-878-GC is 25.2 ± 3.8 wt.% (1 SD, n = 82), ranging between 19.1 and 33.9 wt.%, except for one outlier at ~ 1,750 C.E. with a content of 42.0 wt.% (Fig. 6 and Supplementary Table S5). The quartz-to-carbonate ratio, which represents the siliciclastic-to-carbonate mineral ratios in Hornsund after Görlich (1986) (for details, see section *Potential Sediment Sources in Hornsund*), shows a general upward-increasing trend. In this study, carbonate minerals are defined as the sum of calcite and dolomite (Görlich, 1986).

The contents of Fe-(oxyhydr)oxides range between 0 to 5.98 wt.%. They are generally almost absent throughout the entire core, as also reflected in the average content of 0.3 ± 1.0 wt.% (1 SD, n = 82) (Fig. 6 and Supplementary Table S5). Nevertheless, three prominent peaks are observed at ~ 1,750 C.E., ~ 1,200 C.E., and ~ 910 C.E..

DISCUSSION

Stratigraphy

In this study, we defined three stratigraphic units in core HH19-878-GC based on their respective geochemical and lithological characteristics, and age (Fig. 2). Unit A, which extends from the core base to 200 cm, was deposited between 4.9 kyr B.P. and ~ 790 C.E., covering the period from the latest stage of the middle Holocene to the early stage of the late Holocene. This unit is characterized by a general rise in detrital ε_{Nd} values and is composed predominantly of bioturbated sandy mud with horizontal burrows. Mean grain size is generally the largest among the stratigraphic units (average 11.2 ± 2.2 μm, 1 SD, n = 41) and tends to decrease upward. In contrast, while IRD is rarely recognized at the base, scattered outsized clasts and an IRD layer (e.g., ~310 cm) become more apparent in the upper part of the unit.

Unit B, defined from 200 to 80 cm (~ 790 to 1,470 C.E.), predominantly corresponds to the Medieval Warm Period (MWP). This unit shows significant fluctuations in detrital ε_{Nd} values, with three maximum peaks reaching as high as -12.5 (Fig. 2). This unit comprises primarily sandy mud, characterized by the alteration of massive and bioturbated zones with thin vertical tubes. Unit B shows a general reduction in mean grain size compared to Unit A, mainly due to higher clay contents, with an average of 8.2 ± 1.1 μm (1 SD, n = 24). Notably, the sand content fluctuates largely between 5.8 and 44.8 wt.% (average 16.7 ± 12.0 wt.%, 1 SD, n = 12), marked by two prominent peaks. Additionally, numerous coarse clasts, especially IRD-enriched layers, are frequently identified in Unit B.

Unit C, located between 80 cm and the core top (after 1,470 C.E.), was deposited mainly during and after the Little Ice Age (LIA) (Fig. 2). In this unit, detrital ε_{Nd} values are generally lower compared to the other units, reaching as low as -15.5. Unit C consists of bioturbated sandy mud with vertical tubes. There is no significant change in mean grain size, which ranges between 7.4 and 8.2 μm (8.2 ± 0.6, 1 SD, n = 17). Some coarse clasts are sporadically identified, generally decreasing in number towards the top.

Potential Sediment Sources in Hornsund

The reconstruction of sediment provenance changes in polar regions can provide unique insights into past glacier configurations, given the close relationship between regional sediment supply and glacial activity (e.g., Farmer et al., 2006; Phillips and Grantz, 2001). Here, we use detrital ε_{Nd} values and bulk mineral assemblages to trace provenance variations downcore and their link to glacial activity in Hornsund for the past c. 4.9 kyr. The detrital ε_{Nd} of bulk sediments is particularly useful for fingerprinting different sediment sources eroded from nearby catchment areas via diverse transport pathways and processes (e.g., Horikawa et al., 2015; Jang et al., 2021; Wilson et al., 2018). Given that the diverse bedrock geology around Hornsund may complicate the discriminative use of Nd isotopes for reconstructing provenance, we also use bulk mineral assemblages as source indicators (e.g., Görlich, 1986; Jang et al., 2021; Vogt and Knies, 2009). In particular, ε_{Nd} values and bulk mineral assemblages from surface sediments, especially those collected near glacier fronts or sediment outlets, serve as the representative value of each source region (i.e., end-member) (e.g., Horikawa et al., 2010). This approach is preferred over using bedrock values due to the heterogeneity of Svalbard bedrock and the diversity of their ε_{Nd} values, within a single catchment area (Hindshaw et al., 2018; Jang et al., 2020).

The sub-basins of Hornsund (i.e., Brepollen, Samarinvågen, Austre and Vestre Burgerbukta, and Isbjörnhamna) are currently affected by tidewater glaciers, thereby serving as primary depocenters for terrigenous sediments (Fig. 1). As a result, each sub-basin is typically recognized as a single-source basin, influenced predominantly by suspension settling from local meltwater plumes (Görlich, 1988; Moskalik et al., 2018). In contrast, in the ice-distal location of the main basin, sediment composition is governed by the mixing of sedimentary materials from various sources, each represented by individual sub-basins in conjunction with external inputs drained into the fjord (Görlich, 1986). In this context, proxy records for provenance in fjord surface sediments can be used to establish the geochemical characteristics of each source.

A compilation of detrital ε_{Nd} values for surface sediments in Hornsund based on previous data (Jang et al., 2020; Kim et al., 2023) illustrates basin-specific geochemical variability (Fig. 7A), which we use to identify three potential source areas (A, B, and C) for Hornsund sediments.

1) Group A represents the innermost source, distinguished by significantly high detrital ε_{Nd} values. This source is expressed in the surface sediments of Brepollen, the innermost part of Hornsund, exhibiting detrital ε_{Nd} values as high as -10.1 (Fig. 7A). The predominance of Mesozoic and Cenozoic sedimentary rocks in the outcrops surrounding Brepollen (Dallmann and Elvevold, 2015) indicates their presumed role as primary source rocks. This inference could be further supported by similarly higher ε_{Nd} values in the surface sediments of Storfjorden, where catchment areas are dominated by similar rock formations (Dallmann and Elvevold, 2015) (Fig. 7A).

2) Group B is defined as the central source, identified primarily by detrital ε_{Nd} in surface sediments from Hornsund central sub-basins, such as Samarinvågen, Austre Burgerbukta, and Vestre Burgerbukta. In general, the detrital ε_{Nd} in these regions is lower, reaching values as low as -24.9 near the glacier front in Vestre Burgerbukta (Fig. 7A). Despite a higher detrital ε_{Nd} value of -12.8 near the glacier front in Austre Burgerbukta, the detrital ε_{Nd} values of surface sediments in the region where the sediment inputs from Austre and Vestre Burgerbukta merge are notably lower, ranging from -23.7 to -20.7 (Fig. 7A). This observation implies minor sediment contribution from Austre Burgerbukta to the main basin, suggesting that Group B sediments are mostly tagged with relatively lower ε_{Nd} values. Considering the geology of bedrock terranes adjacent to central Hornsund sub-basins, Group B sediments are most likely derived from the erosion of Paleozoic sedimentary rocks, including Cambrian and Ordovician carbonate rocks (Dallmann and Elvevold, 2015).

3) Group C is characterized by high ε_{Nd} values, whose provenance is inferred from a general seaward detrital ε_{Nd} increase of surface sediments from the main basin to the outer fjord. Notably, the detrital ε_{Nd} value in the outer fjord exceeds the core-top value at site HH19-878-GC by 2-epsilon (ε) units, providing a distinctive marker for identification (Fig. 7A). Considering the prevailing eastward oceanic current along the southern coast governed by the Coriolis force (Jakacki et al., 2017; Pawłowska et al., 2017), it is likely that sediments with radiogenic detrital ε_{Nd} signatures can be transported from outside Hornsund into the main basin by surface water circulation, thereby contributing to the advection of sediments carrying higher detrital ε_{Nd} values. While the potential source rocks of Group C remain uncertain, the prevailing oceanic current following coastal lines may point towards late Paleozoic to Mesozoic sedimentary rocks in the southwestern catchments of Hornsund.

Mineralogical abundances can further improve our ability to discriminate between potential sediment sources, in particular between Group A and Group C, which are both characterized by relatively high ε_{Nd} values. Previous investigations on sediment mineralogy in Hornsund have revealed basin-specific mineralogical features, such as a quartz-feldspar province in Brepollen and a carbonate-feldspar province in the outer fjord (Görlich, 1986). In this context, we explore the spatial variability of quartz-to-carbonate ratios in Hornsund surface sediments (data from Görlich, 1986; Jang et al., 2023; Vogt and Jang, 2023) (Fig. 7B). The surface sediments in Brepollen show high quartz-to-carbonate ratios, ranging between approximately 14 and 327, significantly surpassing the ratios in the outer fjord ranging from about 1.9 to 5.3. Such a stark contrast between the ratios in the representative depocenters affected by Groups A and C highlights that quartz-to-carbonate ratios effectively complement the use of detrital ε_{Nd} for tracing sediment provenance.

It is important to note that the Isbjörnhamna catchment area could also serve as a source of sediment in Hornsund, as inferred from its large estimated sediment yield of approximately 2,000 t km^{-2} yr^{-1} (Moskalik et al., 2018). However, the absence of any detrital ε_{Nd} data for surface sediments in Isbjörnhamna makes it challenging to determine whether this new source can be integrated into adjacent source groups like Groups B and C, or if it should be classified as a distinctive end-member. An early investigation of sediment mineralogy in Isbjörnhamna (Görlich, 1986) demonstrated that the surface sediments in Isbjörnhamna exhibited relatively low carbonate contents, mostly reflecting the absence of carbonate rocks in the surrounding catchment areas. As a result, the quartz-to-carbonate ratios of surface sediments in inner Isbjörnhamna (6.8 ± 2.6, 1 SD, n = 4) tend to be higher than those for Samarinvågen (1.7 ± 0.4, 1 SD, n = 4), Vestre Burgerbukta (1.8 ± 0.3, 1 SD, n = 4) and the outer fjord (3.6 ± 2.4, 1 SD, n = 2) (data from Görlich, 1986; Jang et al., 2023; Vogt and Jang, 2023) (Fig. 7B). This particular mineralogical feature suggests that the Isbjörnhamna catchment can be considered as a distinctive potential source (Group D) in this study, even though its corresponding detrital ε_{Nd} value remains uncertain.

To summarize, we identify four potential sources for Hornsund sediments. Firstly, the Brepollen catchment area is proposed as the innermost source (Group A), with relatively high detrital ε_{Nd} values (up to -10.1) and quartz-to-carbonate ratios (up to 327; Fig. 8). Secondly, the catchment areas around Vestre Burgerbukta and Samarinvågen correspond to the central sources (Group B), supplying sediments with unradiogenic detrital ε_{Nd} values (as low as -24.9) and low quartz-to-carbonate ratios (down to ~ 1; Fig. 8). Thirdly, sediments can also be transported by advected oceanic inflow from outside the fjord (Group C). This outermost and external source is characterized by a relatively higher detrital ε_{Nd} value of -11.9 and a low to intermediate quartz-to-carbonate ratio (3.6 ± 2.4, 1 SD, n = 2) (Fig. 8). Lastly, the Isbjörnhamna catchment can also be considered a local source (Group D) associated with carbonate-depleted sediments, hence with intermediate to high quartz-to-carbonate ratios compared to Groups B and C (Fig. 8).

Changes in Sediment Sources at Site HH19-878-GC over the Last 4.9 kyr

The variability of detrital ε_{Nd} in core HH19-878-GC over the last 4.9 kyr does not strongly correlate with quartz-to-carbonate ratios (Fig. 9), possibly reflecting various mixing processes between multiple sources and/or the potential influence of grain size on sediment composition (Görlich, 1988). Nevertheless, the collective insights gained from both proxy records are used below to infer the provenance of sediments deposited at site HH19-878-GC.

Initially, the innermost region (Group A) with high quartz-to-carbonate ratios can be excluded as a potential sediment source at site HH19-878-GC. The quartz-to-carbonate ratios at this site fall predominantly within the range of 1.0 to 6.1, with a single outlier reaching up to 12.6 around 1,750 C.E. (3.0 ± 1.6, 1 SD, n = 82). These mineralogical ratios closely align with the expected ranges from three potential sources situated around the central to the outer fjord (i.e., Groups B, C, and D). On the other hand, the quartz-to-carbonate ratios at site HH19-878-GC are an order of magnitude lower than those found in surface sediments in Brepollen, despite certain paired detrital ε_{Nd} values being comparable to those observed in the same sediments (Fig. 8). This comparative analysis of measured bulk mineralogy strongly suggests that the innermost region (Group A) played a minor role in supplying sediment to site HH19-878-GC over the last 4.9 kyr. Despite evidence that the glaciers around Brepollen have retreated rapidly over the last decades (e.g., Błaszczyk et al., 2019; Saferna et al., 2023) or centuries (e.g., Pälli et al., 2003), their minor contribution to detrital sedimentation at site HH19-878-GC can largely be attributed to the efficient trapping of supplied sediments in the near-source zone, i.e., the glacier front. Indeed, the sedimentation rate in Hornsund tends to decrease exponentially seaward, with the greatest efficiency of sediment removal in tidewater-glacier systems (Görlich, 1986; Görlich et al., 1987). A minor fraction of sediments originating from the inner Hornsund may survive beyond the near-source zone; however, their influence on the sediment components at site HH19-878-GC could be further diluted by contributions from more proximal sources around Isbjörnhamna. This interpretation is reinforced by distinctive basin-specific detrital ε_{Nd} patterns and the quartz-to-carbonate ratios in surface sediments (Fig. 7).

Secondly, the overall trend observed in our proxy records proposes that sediment deposition at site HH19-878-GC is influenced primarily by the external (Group C) and local (Group D) regions, with an episodic contribution from central Hornsund (Group B). As mentioned earlier, the detrital ε_{Nd} values at this site indicate significant variability in the upper part of the core, where vertical bioturbation is prevalent. While burrower activity may have partially reworked sediments, potentially contributing to the geochemical fluctuations (e.g., Aller et al., 2010), evidence for both high sedimentation rates and concurrent variability in bulk mineralogy within the same sediment interval suggests that changes in sediment sources are likely to represent the primary cause for the observed saw-tooth ε_{Nd} pattern (Fig. 9). Additionally, despite limited Nd isotope data, the bottom part of the core, influenced by horizontal bioturbation, also exhibits pronounced fluctuations in the quartz-to-carbonate ratio, hence suggestive of multiple shifts in sediment provenance over the last 4.9 kyr, with terrestrial inputs being gradually enhanced in the most recent period (Fig. 9). These trends are consistent with sediment mixing between two primary sources, each characterized either by high detrital ε_{Nd}

and low quartz-to-carbonate ratio or vice versa. In this scenario, Group C from outside Hornsund may contribute to a rise in detrital ε_{Nd} and a reduction in quartz-to-carbonate ratios, thereby establishing itself as one of the primary sources. On the other hand, Group B, in central Hornsund, appears to exert a lesser influence on sediment deposition at site HH19-878-GC. This is because the other primary source in this binary mixing system must be characterized by a relatively lower detrital ε_{Nd} value and a higher quartz-to-carbonate ratio, while Group B has the potential to induce declines in both proxy records. Instead, Group D around Isbjörnhamna emerges as a compelling additional primary source, the only remaining candidate among potential sediment sources in Hornsund (for details, see section *Potential Sediment Sources in Hornsund*). This local source is indeed characterized by an intermediate to high quartz-to-carbonate ratio (Görlich, 1986) and is likely to have relatively lower detrital ε_{Nd} value, which can counterbalance the influence of Group C in this binary mixing system. Nevertheless, we admit that binary mixing does not fully account for the sediment transport system in Hornsund over the last 4.9 kyr. Low detrital ε_{Nd} values were intermittently aligned with low mineralogical ratios at specific time intervals (e.g., ~ 1.5 and ~ 1.0 kyr B.P.; Fig. 9), which suggests episodic sediment transport from central Hornsund. In this context, we focus on assessing the relative sediment contribution not between each source but between internal sources (Groups B and D) and the external source (Group C), based solely on detrital ε_{Nd} values.

Taken together, the downcore evolution of detrital ε_{Nd} at site HH19-878-GC hence indicates a comprehensive shift in sediment provenance in Hornsund over the past 4.9 kyr, transitioning predominantly from marine to terrestrial sources. This interpretation is supported by an upward rise in TOC/N_{org} and a simultaneous decline in $\delta^{13}C_{org}$ at site HH19-878-GC (Fig. 9), which collectively suggest an increasing influx of land-derived terrestrial organic matter relative to marine organic matter (Knies and Martinez, 2009; Winkelmann and Knies, 2005). This evidence from organic proxies further supports enhanced terrestrial meltwater discharge in Hornsund since the middle Holocene.

Reconstruction of Paleoenvironmental Changes in Hornsund Since the Middle Holocene

Middle Holocene (before 4 kyr B.P.).--- The temporal variability in sediment provenance at site HH19-878-GC reflects the overall environmental changes in Hornsund since the middle Holocene. The initial clue for environmental conditions during the latest stage of the middle Holocene can be obtained from the bottom part of Unit A, which is characterized by bioturbated mud deposits with low amounts of IRD. The bioturbated mud unit in Svalbard fjords, including Hornsund, typically represents ice-distal glacimarine sediments (Forwick and Vorren, 2009; Görlich, 1986; Ó Cofaigh and Dowdeswell, 2001). The limited occurrence of IRDs in this unit further suggests lower glacial activity (e.g., Baeten et al., 2010; Forwick and Vorren, 2009; Hald et al., 2004), pointing towards conditions akin to nearly open-marine conditions during the middle Holocene. This period has been recognized not only as the global Holocene thermal maximum (~ 6.5 kyr B.P.; Kaufman and Broadman, 2023), but also as a time when Svalbard glaciers attained their minimum extent or even vanished (Farnsworth et al., 2020; Fjeldskaar et al., 2018; van der Bilt et al., 2015). The development of some marine beaches in the Bogstranda region, situated east of Hansbreen in Hornsund (Fig. 1), indicates glacier retreat linked to sea ingress during the middle Holocene (Lindner and Marks, 1993). This is supported by radiocarbon dating of mollusc shells collected from the Hornbreen forefield in Brepollen, which suggested that glacier recession at that time led to the opening of the glaciated strait between Sørkapp Land and the rest of Spitsbergen (Fig. 1C), facilitating marine environments in

Hornsund during most of the early and middle Holocene, c. 10.9-3.9 kyr B.P. (Osika et al., 2022).

The landward retreat of glaciers in Hornsund, including Hansbreen, would have likely allowed the coast to remain ice-free during the middle Holocene. As a result, the suspension settling and iceberg calving from this terrestrial source would be restricted, thereby resulting in lower clay and poor IRD flux at site HH19-878-GC, respectively (Fig. 9). Consequently, the advected oceanic inflow may have overwhelmed the terrestrial meltwater discharge, potentially contributing to high detrital ε_{Nd} values and low quartz-to-carbonate ratios at site HH19-878-GC during the middle Holocene (Fig. 9).

Neoglacial: early stage of the late Holocene (~ 4 kyr B.P. to ~ 790 C.E.).--- From c. 4 kyr B.P., a noticeable increase in the frequency of IRD was observed from the bottom to the upper part of Unit A. This trend can be attributed to enhanced iceberg calving, suggesting an overall environmental transition toward higher glacial activity during the early stage of the late Holocene. While the potential influence of sea-ice IRD transportation cannot be excluded (e.g., Forwick and Vorren, 2009; Joo et al., 2019), the presence of outsized clasts up to 5 cm in diameter most likely reflects the involvement of icebergs (e.g., Gilbert, 1990; Knies et al., 2001). In this context, the identification of an IRD-enriched layer at 2.2 kyr B.P. may have resulted from the collapse of marine-terminating glaciers (e.g., Elliot et al., 2001), potentially offering empirical evidence for the presence of such glaciers in Hornsund (Figs. 2, 6) (e.g., Elliot et al., 2001).

On this basis, we infer that glaciers in Hornsund began to regrow and expand seaward during the early stage of the late Holocene. This time interval broadly coincides with increased glacial activity in Svalbard during the Neoglacial period (review in Farnsworth et al., 2020), likely caused by summer insolation decline (Laskar et al., 2004) and ocean cooling (Farnsworth et al., 2020; Hald et al., 2004; Rasmussen et al., 2012). Neoglacial glacier growth and readvances have been observed in the northern and western parts of Svalbard, including the catchment areas of Linnévatnet (Svendsen and Mangerud, 1997) and Hajeren lakes (van der Bilt et al., 2015), as well as Billefjorden (Baeten et al., 2010) and Tempelfjorden (Forwick et al., 2010). Similarly, in Hornsund, the widespread glacial advance has been well documented through age determinations of outwash sands, tills, and moraines across the region (Lindner and Marks, 1993; Lindner et al., 1984). The absence of dated mollusc shells from 3.9 to 1.3 kyr B.P. in the terrestrial parts of Hornbreen forefield also suggests a potential reclosure of the glaciated strait between Sørkapp Land and the rest of Spitsbergen in Brepollen (Osika et al., 2022), providing additional support for the Neoglacial glacier readvance in the Hornsund region.

Independent support can be derived from the application of Fe-(oxyhydr)oxides as a proxy for meltwater discharge events from adjacent glaciers (Jang et al., 2023) (Fig. 9). Interestingly, the abundance of Fe-(oxyhydr)oxide minerals at site HH19-878-GC peaked around 2.2 kyr B.P., albeit in small quantities. As glacially derived iron accumulates primarily at the interface between meltwater and seawater (Boyle et al., 1977; Raiswell et al., 2018; Schroth et al., 2014; Zhang et al., 2015), these modest enrichments potentially indicate that glacier fronts extended closer to the study site after the middle Holocene, at least until 2.2 kyr B.P..

Collectively, we suggest that enhanced glacial activity prevailed in Hornsund during the Neoglacial period, particularly linked to the development of marine-terminating glaciers. This transition would have led to increased contribution of terrestrial meltwater discharge, explaining the overall decrease in both detrital ε_{Nd} and $\delta^{13}C_{org}$, concomitant with higher clay contents (Fig. 9).

Medieval Warm Period: middle stage of the late Holocene (~ 790 to 1,470 C.E.).--- Unit B, spanning approximately from 790 to 1,470 C.E., corresponds broadly to the Medieval Warm Period (MWP). While the MWP is conventionally set between 950 and 1,200 C.E. (Mann et al., 2009; Miller et al., 2010), it is generally considered to encompass the 1,000 to 1,600 C.E. period, especially in Hornsund (Pawłowska et al., 2016). During the MWP, various regions, particularly around the North Atlantic sector of the Arctic, experienced warmer climate conditions compared to the early 20th century (review in Hughes and Diaz, 1994). Although the MWP is not recognized as a global climate event (Broecker, 2001; Hughes and Diaz, 1994), ice-core records from western Svalbard indicate that Svalbard also encountered general warmth before 1,200 C.E., comparable to the late 1990s (Divine et al., 2011). Notably, dating investigations of both mollusc shells and moraine boulders have suggested that this warming event most likely contributed to the overall retreat of glaciers in Hornsund inland, leading to the reopening of the glaciated strait in Brepollen from ~ 1.3 kyr B.P. (650 C.E.) to before ~ 0.7 kyr B.P. (1,250 C.E.) (Osika et al., 2022). Similarly, low and stable IRD fluxes at core HF_2011 indicate limited glacial activity in Hornsund between 1,000 and 1,800 C.E. (Pawłowska et al., 2016). The multiple detrital ε_{Nd} maxima observed in Unit B at site HH19-878-GC also support a general glacial retreat inland in Hornsund between 790 and 1,470 C.E. (Fig. 9), with higher ε_{Nd} values being suggestive of enhanced sediment contribution from outer Hornsund brought by regional surface waters relative to glacial sediment delivered by local meltwater discharge.

However, the detrital ε_{Nd} values fluctuated and reached minimum values twice during that interval (Fig. 9), indicating the alternation of successive periods of reduced and enhanced glacial activity. Notably, Unit B of core HH19-878-GC stands for its abundant outsized clasts and IRD-enriched layers, occurring more frequently than in the underlying stratigraphic units (Fig. 2). These findings strongly imply a pattern of marked glacial fluctuations, with alternating advances and retreats of marine-terminating glaciers in Hornsund between 790 and 1,470 C.E.. Fe-(oxyhydr)oxide minerals provide additional evidence for episodic glacial advances. The occurrence of two prominent peaks of Fe-(oxyhydr)oxides slightly precedes the occurrence of low detrital ε_{Nd} values (Fig. 9). These peaks of Fe-(oxyhydr)oxide minerals may have resulted from episodical advances of local glaciers, such as Hansbreen, into deeper waters in Hornsund between 790 and 1,470 C.E. (cf. Jang et al., 2023).

Thus, our finding suggests two scenarios for the development of the glacimarine environments in Hornsund during the MWP. First, the MWP may have persisted for a shorter duration than previously defined in Hornsund (e.g., ~ 1,000 to 1,600 C.E. according to Pawłowska et al., 2016). Alternatively, the warming during this period might not have led to the prevalent glacial retreat in Hornsund. In any case, it is probable that the peak warmth occurred during the interval between two glacial advances, as inferred from the low detrital ε_{Nd} values (i.e., 940 to 1,380 C.E.). Supporting this hypothesis, marine records from core HR-3 (76º57.36' N, 15º12.13' E, water depth 145 m; for location, see Fig. 1) in outer Hornsund reveal significant increases in IRD fluxes at two specific intervals around 1,075 and 1,330 C.E. (Majewski et al., 2009). These IRD peaks coincide with declining $\delta^{18}O$ values of benthic foraminifers, suggesting substantial calving events associated with the advances of Hansbreen glacier into marine environments at those times (Majewski et al., 2009). Likewise, glacier advances or surges have been widely identified in the inner Hornsund around 1,140 C.E. (Marks and Pekala, 1986) and in other Svalbard fjords between approximately 1,060 and 1,430 C.E. (Evans and Rea, 2005; Farnsworth et al., 2017; Hald et al., 2001; Larsen et al., 2018; Lovell et al., 2018; Lyså et al., 2018). Collectively, it is inferred that either the MWP persisted over a short duration, or Svalbard glaciers exhibited a less pronounced response to warmth during that period.

Glacimarine environments in Hornsund between 790 and 1,470 C.E. exhibited significant variability, characterized by rapid fluctuations in glacial dynamics. While glaciers generally retreated landward, including during the peak warmth of the MWP, they also advanced at least twice. These dynamic shifts likely intensified the influence of terrestrial inputs, as evidenced by general low $\delta^{13}C_{org}$ values and high clay contents (Fig. 9).

Little Ice Age and modern: late stage of the late Holocene (after ~ 1,470 C.E.).--- Unit C, deposited over the past ~ 600 years, broadly covers the Little Ice Age (LIA, 1,400-1,700 C.E. from Mann et al., 2009; 1,600-1,900 C.E. from Pawłowska et al., 2016), and the modern period. While Unit C shares similar characteristics with Unit B, IRD is primarily dispersed rather than concentrated into distinct layers (Fig. 2). Glacial activity in Hornsund appears to have persisted at higher levels, influencing sediment deposition at site HH19-878-GC after approximately 1,470 C.E.. The scattered IRD may indicate the potential impact of both marine-terminating glacier calving and sea-ice drifting. However, the prevailing low detrital ε_{Nd} values suggest a greater contribution from local glaciers (i.e., Hansbreen) rather than sea-ice from the Barents-Kara seas ($-8.3 < \varepsilon_{Nd} < -9.4$ from Tütken et al., 2002). A previous investigation on the lithological composition of IRD collected from outer Hornsund yielded a similar conclusion, emphasizing that the IRD in this region originates predominantly from marine-terminating glaciers and, to a small degree, from sea-ice (Majewski et al., 2009). Therefore, in this section, we discuss the environmental reconstruction over the last ~ 600 years, focusing primarily on glacier behavior.

The fluctuations in detrital ε_{Nd} values between -12.5 and -15.5 in Unit C at site HH19-878-GC reveal highly unstable environmental conditions in Hornsund during the last six centuries (Fig. 9). In detail, high detrital ε_{Nd} values at the boundary to Unit B most likely indicate reduced supply of terrigenous sediment due to limited glacial activity in the Hornsund region during or shortly after the MWP. However, detrital ε_{Nd} abruptly decreases thereafter, reaching values as low as -15.5 around 1,580-1,620 C.E. (Fig. 9). This ε_{Nd} shift towards lower values indicates increased sediment supply from the catchment areas around Isbjörnhamna, implying glacial activity peaking during the onset of the LIA. Glaciers such as Hansbreen would have expanded into the fjord basin, consistent with the peak accumulation of Fe-(oxyhydr)oxide minerals following low ε_{Nd} at site HH19-878-GC (e.g., Jang et al., 2023) (Fig. 9). Given the subsequent up-and-down variations in detrital ε_{Nd} values, albeit with smaller variability (Fig. 9), glaciers in Hornsund appear to have experienced retreat and readvance since then. In particular, the second glacial advance over the last ~ 600 years would have occurred around 1,900 C.E., which broadly coincided with the end of the LIA. The most recent increase in detrital ε_{Nd} values appears to correspond with the recent glacial retreat (e.g., Błaszczyk et al., 2019; Pälli et al., 2003). However, it is important to note that supply from terrestrial sources continued.

In summary, glacial dynamics during and after the LIA can be characterized by at least two cycles of retreat and advance. Based on detrital ε_{Nd}, the first glacial advance likely occurred around 1,580-1,620 C.E., followed by the second-largest advance around 1,900 C.E.. These findings are consistent with the multi-step glacial advance recorded in other Svalbard areas during the LIA (Røthe et al., 2015; van der Bilt et al., 2015; Werner, 1993). However, exact timings remain to be determined. High-resolution investigations will offer the potential to precisely reconstruct the intricate glacial dynamics in Hornsund during the LIA.

Changes in Fe-S Cycling in Response to Glacial Dynamics

The origin of authigenic Fe-(oxyhydr)oxide phases in sediments can be inferred from REE abundances and shale-normalized patterns. Leached fractions from riverine and marine sediments worldwide typically display mid-REE enrichments relative to light- and heavy-REE, typically exhibiting CI values between 1.2 and 2.5 (Jang et al., 2024 and references therein). The mid-REE enrichments in leached authigenic fractions reflect their preferential uptake upon Fe-(oxyhydr)oxide precipitation (Martin et al., 2010) and/or the fact that they are sourced from upward-migrating diagenetic fluids enriched in mid-REE in the marine environment (Haley et al., 2004). However, authigenic fractions leached from sediments draining sedimentary basins dominated by black shales (Bayon et al., 2020) or from glacial catchments (Jang et al., 2024) display distinctively higher mid-REE enrichments that depart significantly from CI values for typical marine Fe-(oxyhydr)oxides. Recently, Jang et al. (2024) have shown that such high CI values in Fe-(oxyhydr)oxide fractions from glacial environments were linked to pyrite oxidation following glacial erosion and weathering. Glacial weathering is known to be dominated by the oxidation of sulfide minerals (Torres et al., 2017). Following glacial erosion and oxidative sulfide weathering, the release of sulfuric acid can drive the preferential dissolution of apatite, a mid-REE-enriched phosphate mineral. The resulting Fe-(oxyhydr)oxide phases, precipitated from glacial meltwaters, may incorporate a characteristic mid-REE-enriched signature (Jang et al., 2024). The CI values in leached fjord sediments can hence be used to infer glacial activity and related chemical weathering processes in surrounding catchments.

At site HH19-878-GC, the CI values of authigenic sediments vary between 3.0 and 4.6 (Fig. 9), markedly surpassing the typical range observed in leached sediments worldwide, as well as those of corresponding detrital sediments (CI ~ 1; Fig. 5). As discussed above, such high CI values exceeding 2.5 are found exclusively in leached fractions of sediments derived from watersheds dominated by intense sulfide weathering (Bayon et al., 2020; Jang et al., 2024). Therefore, at site HH19-878-GC, these mid-REE enrichments are clearly related to sulfide oxidation and the subsequent precipitation of glacially derived Fe-(oxyhydr)oxide phases that can be transported to the marine environment. Likewise, core HH17-1085-GC retrieved from the continental shelf off northern Svalbard also displays high CI values, ranging between 2.3 and 3.8 (average CI ~ 2.8 ± 0.3, 1 SD, n = 29; Jang et al., 2024).

In Hornsund, the most prominent peaks in CI values occurred during the MWP and the LIA (Fig. 9). A broad positive correlation between detrital ε_{Nd} and CI values since the MWP (r = 0.48, n = 17) could imply that the observed increase in CI values coincided with a shift in provenance involving higher contribution from sulfide-bearing shale deposits. However, before the MWP, CI values remain relatively stable despite of varying detrital ε_{Nd} values at site HH19-878-GC. Thus, we propose instead that the observed CI increase during the MWP and LIA is related to accelerated sulfide oxidation linked with more intense glacial weathering (understood as chemical weathering in glacial catchments; cf. Jang et al., 2020). Rapid glacial advances likely played a key role in this scenario, triggering active glacial abrasion and subsequent widespread exposure of newly eroded rock substrates (e.g., Calmels et al., 2007; Stachnik et al., 2022). A similar case can be found in core HH17-1085-GC from the continental shelf off northern

Svalbard, albeit with lower temporal resolution for CI values (n = 29 over the last 16.3 kyr; Jang et al., 2024). In this core, significant increases in CI values occurred exclusively during the late Holocene, coinciding with glacier readvances (Jang et al., 2021). Since coal mining in Svalbard began in the early 1900s, acid mine drainage may have also contributed to significant mid-REE enrichment (Jang et al., 2024), possibly coinciding with the second, more recent, CI peak during the LIA (Fig. 9). Although most coal mining activities in Svalbard took place around Isfjorden, Kongsfjorden, and Van Mijenfjorden–areas distant from Hornsund–the extraordinary high TOC/N_{org} ratio, reaching up to 43, could hint at the possibility that yet unknown coal mining activity occurred in adjacent areas or that remote transport pathways of mining-related particulates episodically influenced local sedimentation (cf. Winkelmann and Knies, 2005), hence supporting the influence of anthropogenic impact on the observed high CI values in modern era. We acknowledge that bioturbation (as evidenced by the presence of vertical tubes in Units B and C at site HH19-878-GC) may possibly have contributed, at least partly, to the observed CI increase, by promoting diagenetic sulfide oxidation (Canfield et al., 1993; Thamdrup et al., 1994; Wehrmann et al., 2014; Wehrmann et al., 2017). However, despite intense vertical bioturbation in the modern period (Fig. 2), CI values tend to decrease (Fig. 9), likely in response to recent glacier retreat (e.g., Błaszczyk et al., 2019; Pälli et al., 2003). Therefore, we conclude that the observed CI increase since the MWP was driven primarily by enhanced glacial weathering.

The inferred relationship between sulfide oxidation and glacial activity has implications for the future evolution of sulfur and other bioessential elements in the Arctic coastal environments. Over the past decades, Svalbard glaciers have significantly retreated, as evidenced by negative glacier mass balance (Hagen et al., 2003) and/or the reduced glaciated area (Nuth et al., 2013). The recent acceleration of glacier mass loss (Kohler et al., 2007; Zemp et al., 2019) suggests that many marine-terminating glaciers in Svalbard will eventually become land-terminating glaciers in the near future. Drawing an analogy to the diminished CI values during the middle Holocene when the tidewater glaciers mostly disappeared in Hornsund, a potential shift from marine to land-terminating glaciers in the near future may reduce the bioessential elemental input driven by sulfide oxidation associated with glacial weathering, with negative feedbacks in marine ecosystems (Jørgensen et al., 2021). Further investigations is required to fully understand the implications of such environmental changes on sub-Arctic marine ecosystems and biogeochemical processes.

CONCLUSIONS

In this study, we present multi-proxy records from an approximately 400-cm-long sediment core retrieved from outer Hornsund. This core enables us to reconstruct environmental changes over the past 4,900 years, including nearly open-marine conditions during the middle Holocene, the gradual formation of marine-terminating glaciers during the Neoglacial period (~ 4,000 years B.P. to 790 C.E.), rapid glacial fluctuations during the MWP and LIA, and currently ongoing deglaciation. Additionally, the use of REE in authigenic sediments indicates significant mid-REE enrichments in Hornsund, which we attribute to prevailing sulfide oxidation driven by glacial weathering in surrounding catchments. Our REE data show that enhanced pyrite oxidation occurred during glacial advances, such as during specific intervals of the MWP and LIA. Assuming parallel conditions between the middle Holocene and future climate projections, we infer that sulfide oxidation and associated nutrient fluxes into Arctic coastal environments will weaken in the future in response to reduced glacier extent. Further paleoenvironmental investigations in Hornsund are needed to improve our understanding and predictive capabilities regarding future environmental responses to ongoing climate warming.

ACKNOWLEDGMENTS

This study was supported by the National Research Foundation of Korea (NRF) grant funded by the Korea Government (MSIT)(NRF-2021M1A5A1075512, NRF-2017R1A6A1A07015374, and RS-2024-00336841). We would like to thank all the participants of the cruises on RV *Helmer Hanssen* for their support of the core sampling, as well as D. Kim, Y. Son, and I. Nam for laboratory assistance. C.V. thanks the XRD lab team (J. Birkenstock, E.M. Schmidt, R.X. Fischer) for smoothly running the XRD machines. M.-L. Rouget is warmly thanked for assistance during ICP-MS analyses in Brest. Lastly, we appreciate the Editor and two anonymous reviewers for their constructive feedbacks on this manuscript.

DATA AVAILABILITY

The data used in the study can be found in five supplementary tables and are also available in the Korea Polar Data Center via doi:10.22663/KOPRI-KPDC-00002463 with permission.

REFERENCES

Aller, R.C., Madrid, V., Chistoserdov, A., Aller, J.Y., and Heilbrun, C., 2010, Unsteady diagenetic processes and sulfur biogeochemistry in tropical deltaic muds: implications for oceanic isotope cycles and the sedimentary record: Geochimica et Cosmochimica Acta, v. 74, no. 16, p. 4671-4692.

Anderson, S.P., Drever, J.I., Frost, C.D., and Holden, P., 2000, Chemical weathering in the foreland of a retreating glacier: Geochimica et Cosmochimica Acta, v. 64, no. 7, p. 1173-1189.

Baeten, N.J., Forwick, M., Vogt, C., and Vorren, T.O., 2010, Late Weichselian and Holocene sedimentary environments and glacial activity in Billefjorden, Svalbard, *in* Howe, J.A., Austin, W.E.N., Forwick, M. and Paetzel, M., eds., Fjord Systems and Archives: Geological Society of London, Special Publication 344, no. 1, p. 207-223.

Barrat, J., Keller, F., Amossé, J., Taylor, R., Nesbitt, R., and Hirata, T., 1996, Determination of rare earth elements in sixteen silicate reference samples by ICP-MS after Tm addition and ion exchange separation: Geostandards Newsletter, v. 20, no. 1, p. 133-139.

Bartels, M., Titschack, J., Fahl, K., Stein, R., Seidenkrantz, M.-S., Hillaire-Marcel, C., and Hebbeln, D., 2017, Atlantic Water advection vs. glacier dynamics in northern Spitsbergen since early deglaciation: Climate of the Past, v. 13, no. 12, p. 1717-1749.

Bayon, G., Barrat, J.A., Etoubleau, J., Benoit, M., Bollinger, C., and Révillon, S., 2009, Determination of rare earth elements, Sc, Y, Zr, Ba, Hf and Th in geological samples by ICP-MS after Tm addition and alkaline fusion: Geostandards and Geoanalytical Research, v. 33, no. 1, p. 51-62.

Bayon, G., Lambert, T., Vigier, N., De Deckker, P., Freslon, N., Jang, K., Larkin, C.S., Piotrowski, A.M., Tachikawa, K., Thollon, M., and Tipper, E.T., 2020, Rare earth element and neodymium isotope tracing of sedimentary rock weathering: Chemical Geology, v. 553, no. 119794.

Bayon, G., Toucanne, S., Skonieczny, C., Andre, L., Bermell, S., Cheron, S., Dennielou, B., Etoubleau, J., Freslon, N., Gauchery, T., Germain, Y., Jorry, S.J., Menot, G., Monin, L., Ponzevera, E., Rouget, M.L., Tachikawa, K., and Barrat, J.A., 2015, Rare earth elements and neodymium isotopes in world river sediments revisited: Geochimica et Cosmochimica Acta, v. 170, p. 17-38.

Beszczynska-Moller, A., Weslawski, J., Walczowski, W., and Zajaczkowski, M., 1997, Estimation of glacial meltwater discharge into Svalbard coastal waters: Oceanologia, v. 39, no. 3, p. 289-298.

Blaauw, M., and Christen, J.A., 2011, Flexible paleoclimate age-depth models using an autoregressive gamma process: Bayesian analysis, v. 6, no. 3, p. 457-474.

Błaszczyk, M., Ignatiuk, D., Uszczyk, A., Cielecka-Nowak, K., Grabiec, M., Jania, J.A., Moskalik, M., and Walczowski, W., 2019, Freshwater input to the Arctic fjord Hornsund (Svalbard): Polar research, v. 38, no. 3506.

Błaszczyk, M., Jania, J., and Kolondra, L., 2013, Fluctuations of tidewater glaciers in Hornsund Fjord (Southern Svalbard) since the beginning of the 20th century, v. 34, no. 4, p. 327-352.

Blott, S.J., and Pye, K., 2001, GRADISTAT: a grain size distribution and statistics package for the analysis of unconsolidated sediments: Earth Surface Processes and Landforms, v. 26, no. 11, p. 1237-1248.

Boyle, E., Edmond, J., and Sholkovitz, E., 1977, The mechanism of iron removal in estuaries: Geochimica et Cosmochimica Acta, v. 41, no. 9, p. 1313-1324.

Braconnot, P., Harrison, S.P., Kageyama, M., Bartlein, P.J., Masson-Delmotte, V., Abe-Ouchi, A., Otto-Bliesner, B., and Zhao, Y., 2012, Evaluation of climate models using palaeoclimatic data: Nature Climate Change, v. 2, no. 6, p. 417-424.

Broecker, W. S., 2001, Was the medieval warm period global?: Science, v. 291, no. 5508, p. 1497-1499.

Calmels, D., Gaillardet, J., Brenot, A., and France-Lanord, C., 2007, Sustained sulfide oxidation by physical erosion processes in the Mackenzie River basin: Climatic perspectives: Geology, v. 35, no. 11, p. 1003-1006.

Canfield, D.E., Jørgensen, B.B., Fossing, H., Glud, R., Gundersen, J., Ramsing, N.B., Thamdrup, B., Hansen, J.W., Nielsen, L.P., and Hall, P.O.J., 1993, Pathways of organic carbon oxidation in three continental margin sediments: Marine Geology, v. 113, no. 1, p. 27-40.

Dallmann, W., and Elvevold, S., 2015, Bedrock Geology: Geoscience Atlas of Svalbard, Norsk Polarinstitutt, Tromsø, v. 148, p. 133-173.

Diffenbaugh, N.S., Singh, D., Mankin, J.S., Horton, D.E., Swain, D.L., Touma, D., Charland, A., Liu, Y., Haugen, M., Tsiang, M., and Rajaratnam, B., 2017, Quantifying the influence of global warming on unprecedented extreme climate events: Proceedings of the National Academy of Sciences (USA), v. 114, no. 19, p. 4881-4886.

Divine, D., Isaksson, E., Martma, T., Meijer, H.A., Moore, J., Pohjola, V., van de Wal, R.S., and Godtliebsen, F., 2011, Thousand years of winter surface air temperature variations in Svalbard and northern Norway reconstructed from ice-core data: Polar Research, v. 30, no. 1, p. 7379.

Elliot, M., Labeyrie, L., Dokken, T., and Manthé, S., 2001, Coherent patterns of ice-rafted debris deposits in the Nordic regions during the last glacial (10–60 ka): Earth and Planetary Science Letters, v. 194, no. 1, p. 151-163.

Evans, D.J.A., and Rea, B.R., 2005, Late Weichselian deglaciation and sea level history of St Jonsfjorden, Spitsbergen: A contribution to ice sheet reconstruction: Scottish Geographical Journal, v. 121, no. 2, p. 175-201.

Farmer, L.G., Licht, K., Swope, R.J., and Andrews, J., 2006, Isotopic constraints on the provenance of fine-grained sediment in LGM tills from the Ross Embayment, Antarctica: Earth and Planetary Science Letters, v. 249, no. 1, p. 90-107.

Farnsworth, W.R., Allaart, L., Ingólfsson, Ó., Alexanderson, H., Forwick, M., Noormets, R., Retelle, M., and Schomacker, A., 2020, Holocene glacial history of Svalbard: Status, perspectives and challenges: Earth-Science Reviews, v. 208, no. 103249.

Farnsworth, W.R., Ingólfsson, Ó., Noormets, R., Allaart, L., Alexanderson, H., Henriksen, M., and Schomacker, A., 2017, Dynamic Holocene glacial history of st. Jonsfjorden, Svalbard: Boreas, v. 46, no. 3, p. 585-603.

Fjeldskaar, W., Bondevik, S., and Amantov, A., 2018, Glaciers on Svalbard survived the Holocene thermal optimum: Quaternary Science Reviews, v. 199, p. 18-29.

Flink, A.E., Hill, P., Noormets, R., and Kirchner, N., 2018, Holocene glacial evolution of Mohnbukta in eastern Spitsbergen: Boreas, v. 47, no. 2, p. 390-409.

Folk, R.L., and Ward, W.C., 1957, Brazos River bar [Texas]: a study in the significance of grain size parameters: Journal of Sedimentary Petrology, v. 27, no. 1, p. 3-26.

Forwick, M., and Vorren, T.O., 2009, Late Weichselian and Holocene sedimentary environments and ice rafting in Isfjorden, Spitsbergen: Palaeogeography, Palaeoclimatology, Palaeoecology, v. 280, no. 1, p. 258-274.

Forwick, M., Vorren, T.O., Hald, M., Korsun, S., Roh, Y., Vogt, C., and Yoo, K.-C., 2010, Spatial and temporal influence of glaciers and rivers on the sedimentary environment in Sassenfjorden and Tempelfjorden, Spitsbergen, *in* Howe, J.A., Austin, W.E.N., Forwick, M. and Paetzel, M., eds., Fjord Systems and Archives: Geological Society of London, Special Publication 344, no. 1, p. 163-193.

Füssel, H.M., 2007, Adaptation planning for climate change: concepts, assessment approaches, and key lessons: Sustainability Science, v. 2, no. 2, p. 265-275.

Gilbert, R., 1990, Rafting in glacimarine environments *in* Dowdeswell, J.A. and Scourse, J.D., eds., Glacimarine Environments: Processes and Sediments: Geological Society of London, Special Publication 53, no. 1, p. 105-120.

Görlich, K., 1986, Glacimarine sedimentation of muds in Hornsund fjord, Spitsbergen: Annales Societatis Geologorum Poloniae, v. 56, no. 3-4, p. 433-477.

Görlich, K., 1988, Micas and texture of the recent muds in Spitsbergen fjords: study of suspension settling: Annales Societatis Geologorum Poloniae, v. 58, no. 1-2, p. 21-52.

Görlich, K., Weslawski, J.M., and Zajaczkowski, M., 1987, Suspension settling effect on macrobenthos biomass distribution in the Hornsund fjord, Spitsbergen: Polar Research, v. 5, no. 2, p. 175-192.

Grabiec, M., Ignatiuk, D., Jania, J.A., Moskalik, M., Głowacki, P., Błaszczyk, M., Budzik, T., and Walczowski, W., 2018, Coast formation in an Arctic area due to glacier surge and retreat: The Hornbreen–Hambergbreen case from Spistbergen: Earth Surface Processes and Landforms, v. 43, no. 2, p. 387-400.

Hagen, J.O., Kohler, J., Melvold, K., and Winther, J.G., 2003, Glaciers in Svalbard: mass balance, runoff and freshwater flux: Polar Research, v. 22, no. 2, p. 145-159.

Hald, M., Dahlgren, T., Olsen, T.-E., and Lebesbye, E., 2001, Late Holocene palaeoceanography in Van Mijenfjorden, Svalbard: Polar Research, v. 20, no. 1, p. 23-35.

Hald, M., Ebbesen, H., Forwick, M., Godtliebsen, F., Khomenko, L., Korsun, S., Olsen, L.R., and Vorren, T.O., 2004, Holocene paleoceanography and glacial history of the West Spitsbergen area, Euro-Arctic margin: Quaternary Science Reviews, v. 23, no. 20-22, p. 2075-2088.

Haley, B.A., Klinkhammer, G.P., and McManus, J., 2004, Rare earth elements in pore waters of marine sediments: Geochimica et Cosmochimica Acta, v. 68, no. 6, p. 1265-1279.

Heaton, T.J., Köhler, P., Butzin, M., Bard, E., Reimer, R.W., Austin, W.E., Ramsey, C.B., Grootes, P.M., Hughen, K.A., and Kromer, B., 2020, Marine20—the marine radiocarbon age calibration curve (0–55,000 cal BP): Radiocarbon, v. 62, no. 4, p. 779-820.

Hindshaw, R.S., Tosca, N.J., Piotrowski, A.M., and Tipper, E.T., 2018, Clay mineralogy, strontium and neodymium isotope ratios in the sediments of two High Arctic catchments (Svalbard): Earth Surface Dynamics, v. 6, no. 1, p. 141-161.

Horikawa, K., Asahara, Y., Yamamoto, K., and Okazaki, Y., 2010, Intermediate water formation in the Bering Sea during glacial periods: Evidence from neodymium isotope ratios: Geology, v. 38, no. 5, p. 435-438.

Horikawa, K., Martin, E.E., Basak, C., Onodera, J., Seki, O., Sakamoto, T., Ikehara, M., Sakai, S., and Kawamura, K., 2015, Pliocene cooling enhanced by flow of low-salinity Bering

Sea water to the Arctic Ocean: Nature Communications, v. 6, doi.org/10.1038/ncomms8587.

Hughes, A.L., Gyllencreutz, R., Lohne, Ø.S., Mangerud, J., and Svendsen, J.I., 2016, The last Eurasian ice sheets–a chronological database and time-slice reconstruction, DATED-1: Boreas, v. 45, no. 1, p. 1-45.

Hughes, M.K., and Diaz, H.F., 1994, Was there a 'Medieval Warm Period', and if so, where and when?: Climatic Change, v. 26, no. 2-3, p. 109-142.

Jacobsen, S.B., and Wasserburg, G.J., 1980, Sm-Nd isotopic evolution of chondrites: Earth and Planetary Science Letters, v. 50, no. 1, p. 139-155.

Jakacki, J., Przyborska, A., Kosecki, S., Sundfjord, A., and Albretsen, J., 2017, Modelling of the Svalbard fjord Hornsund: Oceanologia, v. 59, no. 4, p. 473-495.

Jakobsson, M., Mayer, L.A., Bringensparr, C., Castro, C.F., Mohammad, R., Johnson, P., Ketter, T., Accettella, D., Amblas, D., An, L., Arndt, J.E., Canals, M., Casamor, J.L., Chauché, N., Coakley, B., Danielson, S., Demarte, M., Dickson, M.-L., Dorschel, B., Dowdeswell, J.A., Dreutter, S., Fremand, A.C., Gallant, D., Hall, J.K., Hehemann, L., Hodnesdal, H., Hong, J., Ivaldi, R., Kane, E., Klaucke, I., Krawczyk, D.W., Kristoffersen, Y., Kuipers, B.R., Millan, R., Masetti, G., Morlighem, M., Noormets, R., Prescott, M.M., Rebesco, M., Rignot, E., Semiletov, I., Tate, A.J., Travaglini, P., Velicogna, I., Weatherall, P., Weinrebe, W., Willis, J.K., Wood, M., Zarayskaya, Y., Zhang, T., Zimmermann, M., and Zinglersen, K.B., 2020, The international bathymetric chart of the Arctic Ocean version 4.0: Scientific Data, v. 7, no. 1, p. 176.

Jang, K., Ahn, Y., Joe, Y.J., Braun, C.A., Joo, Y.J., Kim, J.-H., Bayon, G., Forwick, M., Vogt, C., and Nam, S.-I., 2021, Glacial and environmental changes in northern Svalbard over the last 16.3 ka inferred from neodymium isotopes: Global and Planetary Change, v. 201, no. 103483.

Jang, K., Bayon, G., Han, Y., Joo, Y.J., Kim, J.-H., Ryu, J.-S., Woo, J., Forwick, M., Szczuciński, W., Kim, J.-H., and Nam, S.-I., 2020, Neodymium isotope constraints on chemical weathering and past glacial activity in Svalbard: Earth and Planetary Science Letters, v. 542, no. 116319.

Jang, K., Bayon, G., Pourret, O., Joe, Y.J., Kim, J.-H., Byun, E., Forwick, M., León, R., and Nam, S.-I., 2024, A distinctive rare earth element signature for pyrite oxidation and glacial weathering: Chemical Geology, v. 660, no. 122167.

Jang, K., Bayon, G., Vogt, C., Forwick, M., Ahn, Y., Kim, J.-H., and Nam, S.-I., 2023, Non-linear response of glacier melting to Holocene warming in Svalbard recorded by sedimentary iron (oxyhydr)oxides: Earth and Planetary Science Letters, v. 607, no. 118054.

Jang, K., Huh, Y., and Han, Y., 2017, Authigenic Nd isotope record of North Pacific Intermediate Water formation and boundary exchange on the Bering Slope: Quaternary Science Reviews, v. 156, p. 150-163.

Joe, Y.J., Jang, K., Forwick, M., Laberg, J.S., Kong, G.S., Kang, M.-H., Yoon, S.-H., and Nam, S.-I., 2022, Glacial history and depositional environments in little Storfjorden and Hambergbukta of Arctic Svalbard since the younger dryas: Frontiers in Earth Science, v. 10, p. 1-19.

Joo, Y.J., Forwick, M., Park, K., Joe, Y., Son, Y.J., and Nam, S.-I., 2019, Holocene environmental changes in Dicksonfjorden, west Spitsbergen, Svalbard: Polar Research, v. 38, no. 3426.

Jørgensen, B.B., Laufer, K., Michaud, A.B., and Wehrmann, L.M., 2021, Biogeochemistry and microbiology of high Arctic marine sediment ecosystems—Case study of Svalbard fjords: Limnology and Oceanography, v. 66, p. S273-S292.

Karczewski, A., Kostrzewski, A., and Marks, L., 1981, Late Holocene glacier advances in Revdalen, Spitsbergen: Polish Polar Research, v. 2, no. 1-2.

Kaufman, D.S., and Broadman, E., 2023, Revisiting the Holocene global temperature conundrum: Nature, v. 614, no. 7948, p. 425-435.

Kim, D., Kim, J.-H., Ahn, Y., Jang, K., Jung, J.Y., Bae, M., and Nam, S.-I., 2023, Large contributions of petrogenic and aged soil-derived organic carbon to Arctic fjord sediments in Svalbard: Scientific Reports, v. 13, no. 17935.

Knies, J., Kleiber, H.-P., Matthiessen, J., Müller, C., and Nowaczyk, N., 2001, Marine ice-rafted debris records constrain maximum extent of Saalian and Weichselian ice-sheets along the northern Eurasian margin: Global and Planetary Change, v. 31, no. 1-4, p. 45-64.

Knies, J., and Martinez, P., 2009, Organic matter sedimentation in the western Barents Sea region: Terrestrial and marine contribution based on isotopic composition and organic nitrogen content: Norwegian Journal of Geology/Norsk Geologisk Forening, v. 89, p. 79-89.

Kohler, J., James, T.D., Murray, T., Nuth, C., Brandt, O., Barrand, N.E., Aas, H.F., and Luckman, A., 2007, Acceleration in thinning rate on western Svalbard glaciers: Geophysical Research Letters, v. 34, no. 18.

Larsen, E., Lyså, A., Rubensdotter, L., Farnsworth, W.R., Jensen, M., Nadeau, M.J., and Ottesen, D., 2018, Lateglacial and Holocene glacier activity in the Van Mijenfjorden area, western Svalbard: arktos, v. 4, p. 1-21.

Laskar, J., Robutel, P., Joutel, F., Gastineau, M., Correia, A., and Levrard, B., 2004, A long-term numerical solution for the insolation quantities of the Earth: Astronomy and Astrophysics, v. 428, no. 1, p. 261-285.

Laukert, G., Frank, M., Bauch, D., Hathorne, E.C., Rabe, B., von Appen, W.-J., Wegner, C., Zieringer, M., and Kassens, H., 2017, Ocean circulation and freshwater pathways in the Arctic Mediterranean based on a combined Nd isotope, REE and oxygen isotope section across Fram Strait: Geochimica et Cosmochimica Acta, v. 202, p. 285-309.

Lee, H., Calvin, K., Dasgupta, D., Krinner, G., Mukherji, A., Thorne, P., Trisos, C., Romero, J., Aldunce, P., and Barret, K., 2023, Climate change 2023 synthesis report summary for policymakers: Contribution of Working Groups I, II and III to the Sixth Assessment Report of the Intergovernmental Panel on Climate Change, Geneva, Switzerland.

Lindner, L., and Marks, L., 1993, Middle and Late Quaternary evolution of the Hornsund region, south Spitsbergen: Polish Polar Research, v. 14, no. 3, p. 275-292.

Lindner, L., Marks, L., and Pekala, K., 1984, Late Quaternary glacial episodes in the Hornsund region of Spitsbergen: Boreas, v. 13, no. 1, p. 35-47.

Lovell, H., Benn, D.I., Lukas, S., Ottesen, D., Luckman, A., Hardiman, M., Barr, I.D., Boston, C.M., and Sevestre, H., 2018, Multiple Late Holocene surges of a High-Arctic tidewater glacier system in Svalbard: Quaternary Science Reviews, v. 201, p. 162-185.

Lyså, A., Larsen, E.A., Høgaas, F., Jensen, M.A., Klug, M., Rubensdotter, L., and Szczuciński, W., 2018, A temporary glacier-surge ice-dammed lake, Braganzavågen, Svalbard: Boreas, v. 47, no. 3, p. 837-854.

Majewski, W., Szczuciński, W., and Zajączkowski, M., 2009, Interactions of Arctic and Atlantic water-masses and associated environmental changes during the last millennium, Hornsund (SW Svalbard): Boreas, v. 38, no. 3, p. 529-544.

Mann, M.E., Zhang, Z., Rutherford, S., Bradley, R.S., Hughes, M.K., Shindell, D., Ammann, C., Faluvegi, G., and Ni, F., 2009, Global signatures and dynamical origins of the Little Ice Age and Medieval Climate Anomaly: Science, v. 326, no. 5957, p. 1256-1260.

Marks, L., and Pekala, K., 1986, New datings of Quaternary sediments from Bogstranda and Treskelodden, southern Spitsbergen: Bulletin of the Polish Academy of Sciences, Earth Sciences, v. 34, no. 4, p. 419-425.

Martin, E.E., Blair, S.W., Kamenov, G.D., Scher, H.D., Bourbon, E., Basak, C., and Newkirk, D.N., 2010, Extraction of Nd isotopes from bulk deep sea sediments for paleoceanographic studies on Cenozoic time scales: Chemical Geology, v. 269, no. 3-4, p. 414-431.

Miller, G.H., Brigham-Grette, J., Alley, R.B., Anderson, L., Bauch, H.A., Douglas, M.S.V., Edwards, M.E., Elias, S.A., Finney, B.P., Fitzpatrick, J.J., Funder, S.V., Herbert, T.D., Hinzman, L.D., Kaufman, D.S., MacDonald, G.M., Polyak, L., Robock, A., Serreze, M.C., Smol, J.P., Spielhagen, R., White, J.W.C., Wolfe, A.P., and Wolff, E.W., 2010, Temperature and precipitation history of the Arctic: Quaternary Science Reviews, v. 29, no. 15, p. 1679-1715.

Moskalik, M., Ćwiąkała, J., Szczuciński, W., Dominiczak, A., Głowacki, O., Wojtysiak, K., and Zagórski, P., 2018, Spatiotemporal changes in the concentration and composition of suspended particulate matter in front of Hansbreen, a tidewater glacier in Svalbard: Oceanologia, v. 60, no. 4, p. 446-463.

Nordli, Ø., Przybylak, R., Ogilvie, A.E., and Isaksen, K., 2014, Long-term temperature trends and variability on Spitsbergen: the extended Svalbard airport temperature series, 1898–2012: Polar research, v. 33, no. 1, p. 21349.

Nuth, C., Kohler, J., König, M., von Deschwanden, A., Hagen, J.O.M., Kääb, A., Moholdt, G., and Pettersson, R., 2013, Decadal changes from a multi-temporal glacier inventory of Svalbard: The Cryosphere, v. 7, no. 5, p. 1603-1621.

Ó Cofaigh, C., and Dowdeswell, J.A., 2001, Laminated sediments in glacimarine environments: diagnostic criteria for their interpretation: Quaternary Science Reviews, v. 20, no. 13, p. 1411-1436.

Osika, A., Jania, J., and Szafraniec, J.E., 2022, Holocene ice-free strait followed by dynamic Neoglacial fluctuations: Hornsund, Svalbard: The Holocene, v. 32, no. 7, p. 664-679.

Pälli, A., Moore, J.C., Jania, J., and Glowacki, P., 2003, Glacier changes in southern Spitsbergen, Svalbard,1901–2000: Annals of Glaciology, v. 37, p. 219-225.

Pawłowska, J., Zajączkowski, M., Łącka, M., Lejzerowicz, F., Esling, P., and Pawlowski, J., 2016, Palaeoceanographic changes in Hornsund fjord (Spitsbergen, Svalbard) over the last millennium: new insights from ancient DNA: Climate of the Past, v. 12, no. 7, p. 1459-1472.

Pawłowska, J., Zajączkowski, M., Szczuciński, W., Zaborska, A., Kucharska, M., Jernas, P.E., and Forwick, M., 2017, The influence of Coriolis force driven water circulation on the palaeoenvironment of Hornsund (S Spitsbergen) over the last century: Boreas, v. 46, no. 4, p. 737-749.

Petschick, R., Kuhn, G., and Gingele, F., 1996, Clay mineral distribution in surface sediments of the South Atlantic: sources, transport, and relation to oceanography: Marine Geology, v. 130, no. 3-4, p. 203-229.

Philipps, W., Briner, J., Gislefoss, L., Linge, H., Koffman, T., Fabel, D., Xu, S., and Hormes, A., 2017, Late Holocene glacier activity at inner Hornsund and Scottbreen, southern Svalbard: Journal of Quaternary Science, v. 32, no. 4, p. 501-515.

Phillips, R.L., and Grantz, A., 2001, Regional variations in provenance and abundance of ice-rafted clasts in Arctic Ocean sediments: implications for the configuration of late Quaternary oceanic and atmospheric circulation in the Arctic: Marine Geology, v. 172, no. 1-2, p. 91-115.

Pieńkowski, A.J., Husum, K., Furze, M.F.A., Missana, A.F.J.M., Irvalı, N., Divine, D.V., and Eilertsen, V.T., 2022, Revised ΔR values for the Barents Sea and its archipelagos as a pre-requisite for accurate and robust marine-based ^{14}C chronologies: Quaternary Geochronology, v. 68, no. 101244.

Pin, C., and Zalduegui, J.S., 1997, Sequential separation of light rare-earth elements, thorium and uranium by miniaturized extraction chromatography: Application to isotopic analyses of silicate rocks: Analytica Chimica Acta, v. 339, no. 1-2, p. 79-89.

Raiswell, R., Hawkings, J., Elsenousy, A., Death, R., Tranter, M., and Wadham, J., 2018, Iron in glacial systems: speciation, reactivity, freezing behavior, and alteration during transport: Frontiers in Earth Science, v. 6, no. 222.

Rasmussen, T.L., Forwick, M., and Mackensen, A., 2012, Reconstruction of inflow of Atlantic Water to Isfjorden, Svalbard during the Holocene: Correlation to climate and seasonality: Marine Micropaleontology, v. 94, p. 80-90.

Raven, M.D., and Self, P.G., 2017, Outcomes of 12 years of the Reynolds Cup quantitative mineral analysis round robin: Clays and Clay Minerals, v. 65, no. 2, p. 122-134.

Røthe, T.O., Bakke, J., Vasskog, K., Gjerde, M., D'Andrea, W.J., and Bradley, R.S., 2015, Arctic Holocene glacier fluctuations reconstructed from lake sediments at Mitrahalvøya, Spitsbergen: Quaternary Science Reviews, v. 109, p. 111-125.

Saferna, D., Błaszczyk, M., Grabiec, M., and Gądek, B., 2023, Quantifying changes in extent and velocity of the Hornbreen/Hambergbreen glacial system (SW, Spitsbergen) based on timeseries of multispectral satellite imagery: Remote Sensing, v. 15, no. 14, no. 3529.

Salvigsen, O., and Høgvard, K., 2006, Glacial history, Holocene shoreline displacement and palaeoclimate based on radiocarbon ages in the area of Bockfjorden, north-western Spitsbergen, Svalbard: Polar Research, v. 25, no. 1, p. 15-24.

Schroth, A.W., Crusius, J., Hoyer, I., and Campbell, R., 2014, Estuarine removal of glacial iron and implications for iron fluxes to the ocean: Geophysical Research Letters, v. 41, no. 11, p. 3951-3958.

Silva, J.A., and Bremner, J.M., 1966, Determination and isotope-ratio analysis of different forms of nitrogen in soils: 5. Fixed Ammonium: Soil Science Society of America Journal, v. 30, no. 5, p. 587-594.

Stachnik, Ł., Yde, J.C., Krzemień, K., Uzarowicz, Ł., Sitek, S., and Kenis, P., 2022, SEM-EDS and water chemistry characteristics at the early stages of glacier recession reveal biogeochemical coupling between proglacial sediments and meltwater: Science of The Total Environment, v. 835, no. 155383.

Svendsen, J.I., and Mangerud, J., 1997, Holocene glacial and climatic variations on Spitsbergen, Svalbard: The Holocene, v. 7, no. 1, p. 45-57.

Tanaka, T., Togashi, S., Kamioka, H., Amakawa, H., Kagami, H., Hamamoto, T., Yuhara, M., Orihashi, Y., Yoneda, S., Shimizu, H., Kunimaru, T., Takahashi, K., Yanagi, T., Nakano, T., Fujimaki, H., Shinjo, R., Asahara, Y., Tanimizu, M., and Dragusanu, C., 2000, JNdi-1: a neodymium isotopic reference in consistency with LaJolla neodymium: Chemical Geology, v. 168, no. 3, p. 279-281.

Thamdrup, B., Fossing, H., and Jørgensen, B.B., 1994, Manganese, iron and sulfur cycling in a coastal marine sediment, Aarhus bay, Denmark: Geochimica et Cosmochimica Acta, v. 58, no. 23, p. 5115-5129.

Torres, M.A., Moosdorf, N., Hartmann, J., Adkins, J.F., and West, A.J., 2017, Glacial weathering, sulfide oxidation, and global carbon cycle feedbacks: Proceedings of the National Academy of Sciences (USA), v. 114, no. 33, p. 8716-8721.

Trenberth, K.E., Dai, A., van der Schrier, G., Jones, P.D., Barichivich, J., Briffa, K.R., and Sheffield, J., 2014, Global warming and changes in drought: Nature Climate Change, v. 4, no. 1, p. 17-22.

Tütken, T., Eisenhauer, A., Wiegand, B., and Hansen, B.T., 2002, Glacial–interglacial cycles in Sr and Nd isotopic composition of Arctic marine sediments triggered by the Svalbard/Barents Sea ice sheet: Marine Geology, v. 182, no. 3–4, p. 351-372.

van der Bilt, W.G.M., Bakke, J., Vasskog, K., D'Andrea, W.J., Bradley, R.S., and Ólafsdóttir, S., 2015, Reconstruction of glacier variability from lake sediments reveals dynamic Holocene climate in Svalbard: Quaternary Science Reviews, v. 126, p. 201-218.

Vogt, C., and Jang, K., 2023, Bulk mineral assemblage of sediment cores from Svalbard fjords determined via full pattern QXRD [dataset bundled publication]: PANGAEA, doi:10.1594/PANGAEA.955819.

Vogt, C., and Knies, J., 2009, Sediment pathways in the western Barents Sea inferred from clay mineral assemblages in surface sediments: Norwegian Journal of Geology/Norsk Geologisk Forening, v. 89, p. 41-55.

Vogt, C., Lauterjung, J., and Fischer, R.X., 2002, Investigation of the clay fraction (< 2 μm) of the clay minerals society reference clays: Clays and Clay Minerals, v. 50, no. 3, p. 388-400.

Wehrmann, L.M., Formolo, M.J., Owens, J.D., Raiswell, R., Ferdelman, T.G., Riedinger, N., and Lyons, T.W., 2014, Iron and manganese speciation and cycling in glacially influenced high-latitude fjord sediments (West Spitsbergen, Svalbard): Evidence for a benthic recycling-transport mechanism: Geochimica et Cosmochimica Acta, v. 141, p. 628-655.

Wehrmann, L.M., Riedinger, N., Brunner, B., Kamyshny, A., Hubert, C.R.J., Herbert, L.C., Brüchert, V., Jørgensen, B.B., Ferdelman, T.G., and Formolo, M.J., 2017, Iron-controlled oxidative sulfur cycling recorded in the distribution and isotopic composition of sulfur species in glacially influenced fjord sediments of west Svalbard: Chemical Geology, v. 466, p. 678-695.

Weis, D., Kieffer, B., Maerschalk, C., Barling, J., De Jong, J., Williams, G.A., Hanano, D., Pretorius, W., Mattielli, N., and Scoates, J. S., 2006, High-precision isotopic characterization of USGS reference materials by TIMS and MC-ICP-MS: Geochemistry, Geophysics, Geosystems, v. 7, no. 8, p. 1-30, doi:10.1029/2006gc001283.

Werner, A., 1993, Holocene moraine chronology, Spitsbergen, Svalbard: lichenometric evidence for multiple Neoglacial advances in the Arctic: The Holocene, v. 3, no. 2, p. 128-137.

Wilson, D.J., Bertram, R.A., Needham, E.F., van de Flierdt, T., Welsh, K.J., McKay, R.M., Mazumder, A., Riesselman, C.R., Jimenez-Espejo, F.J., and Escutia, C., 2018, Ice loss from the East Antarctic Ice Sheet during late Pleistocene interglacials: Nature, v. 561, no. 7723, p. 383-386.

Wilson, D.J., Piotrowski, A.M., Galy, A., and Clegg, J.A., 2013, Reactivity of neodymium carriers in deep sea sediments: Implications for boundary exchange and paleoceanography: Geochimica et Cosmochimica Acta, v. 109, p. 197-221.

Winkelmann, D., and Knies, J., 2005, Recent distribution and accumulation of organic carbon on the continental margin west off Spitsbergen: Geochemistry, Geophysics, Geosystems, v. 6, no. 9, no. Q09012.

Zemp, M., Huss, M., Thibert, E., Eckert, N., McNabb, R., Huber, J., Barandun, M., Machguth, H., Nussbaumer, S.U., Gärtner-Roer, I., Thomson, L., Paul, F., Maussion, F., Kutuzov, S., and Cogley, J.G., 2019, Global glacier mass changes and their contributions to sea-level rise from 1961 to 2016: Nature, v. 568, no. 7752, p. 382-386.

Zhang, R., John, S.G., Zhang, J., Ren, J., Wu, Y., Zhu, Z., Liu, S., Zhu, X., Marsay, C.M., and Wenger, F., 2015, Transport and reaction of iron and iron stable isotopes in glacial meltwaters on Svalbard near Kongsfjorden: From rivers to estuary to ocean: Earth and Planetary Science Letters, v. 424, p. 201-211.

FIGURES

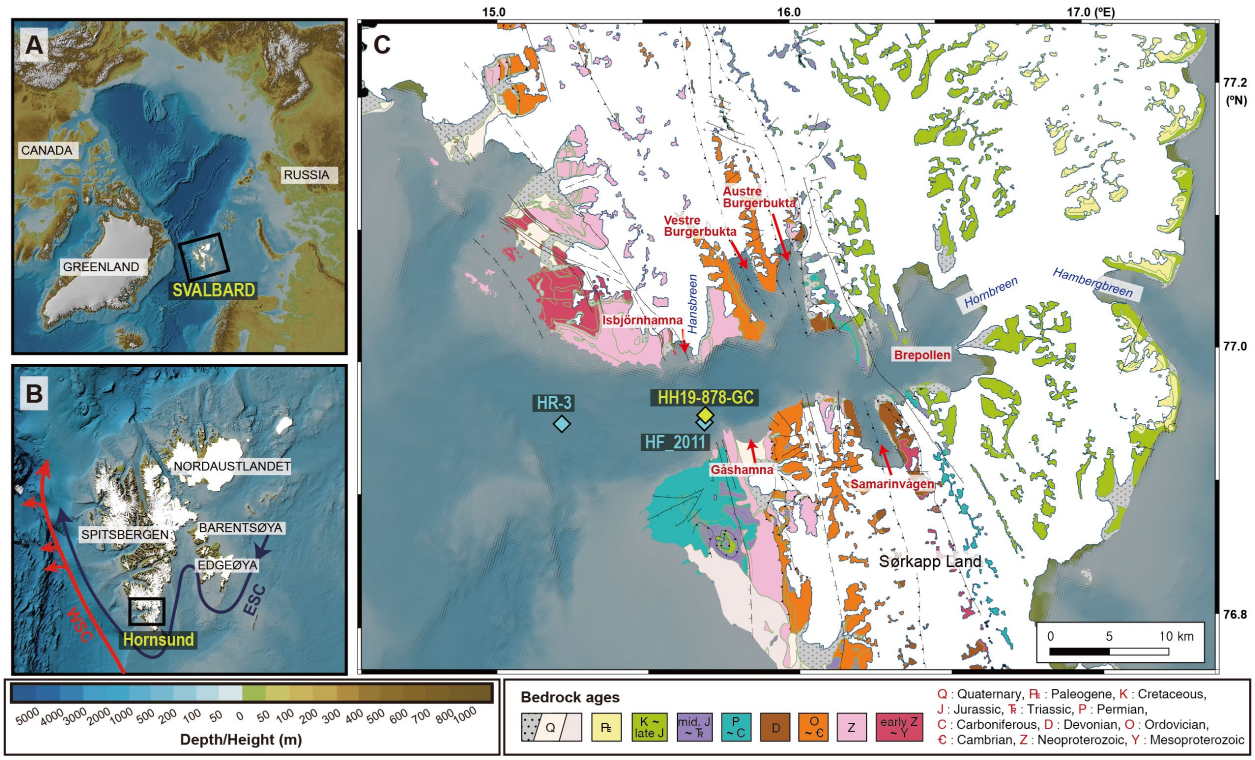

Figure 1. Map of A) the Arctic Ocean, B) Svalbard, and C) Hornsund. The sampling site is marked with a yellow diamond, while comparative sites are indicated with greenish blue diamonds. Various bedrock ages around Hornsund are represented by different colors (Dallmann and Elvevold, 2015). The bathymetric information is based on IBCAO 4.0 bathymetric grid (Jakobsson et al., 2020). Basemap datasets © Norwegian Polar Institute (https://geodata.npolar.no/).

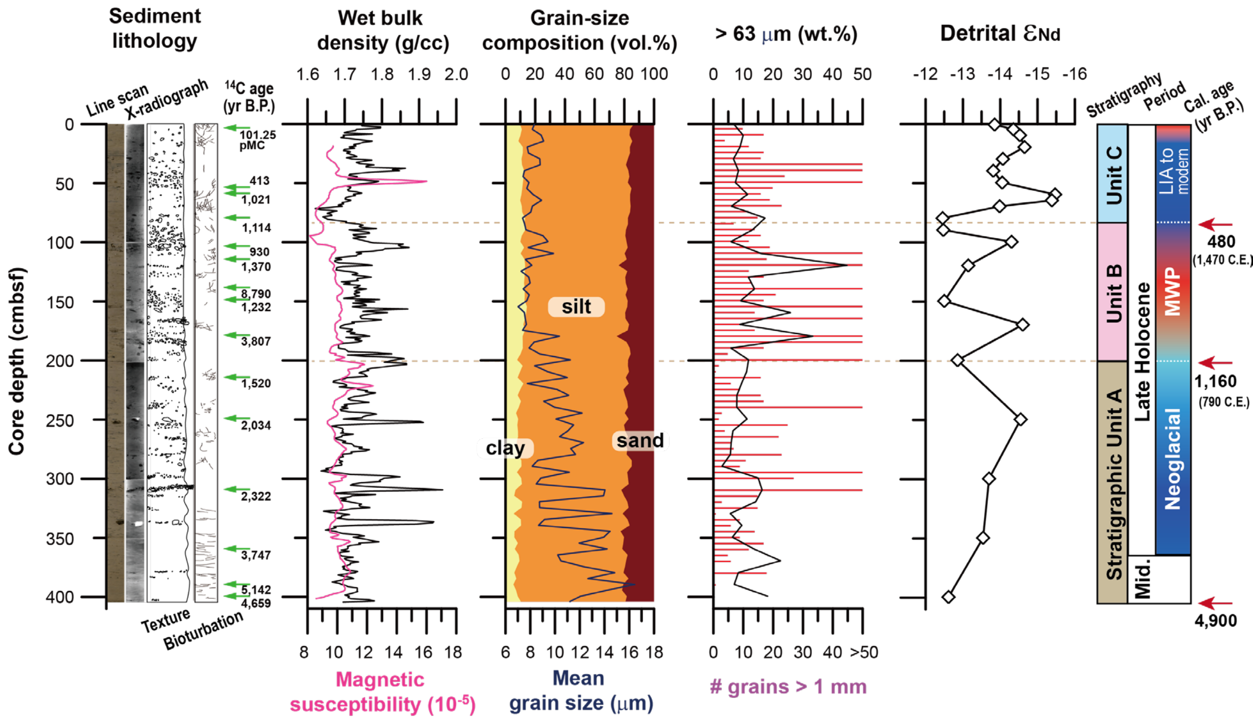

Figure 2. Three stratigraphic units of core HH19-878-GC defined based on lithological and geochemical characteristics, and age. Linescan image, x-radiograph, lithological log, AMS ^{14}C ages (for error, see Table 1), wet bulk density, magnetic susceptibility, grain-size composition, mean grain size, sand fraction (> 63 μm), the number of grains greater than 1 mm, detrital ε_{Nd} values and time period are shown for comparison. Note that the horizontal axis is reversed for detrital ε_{Nd}.

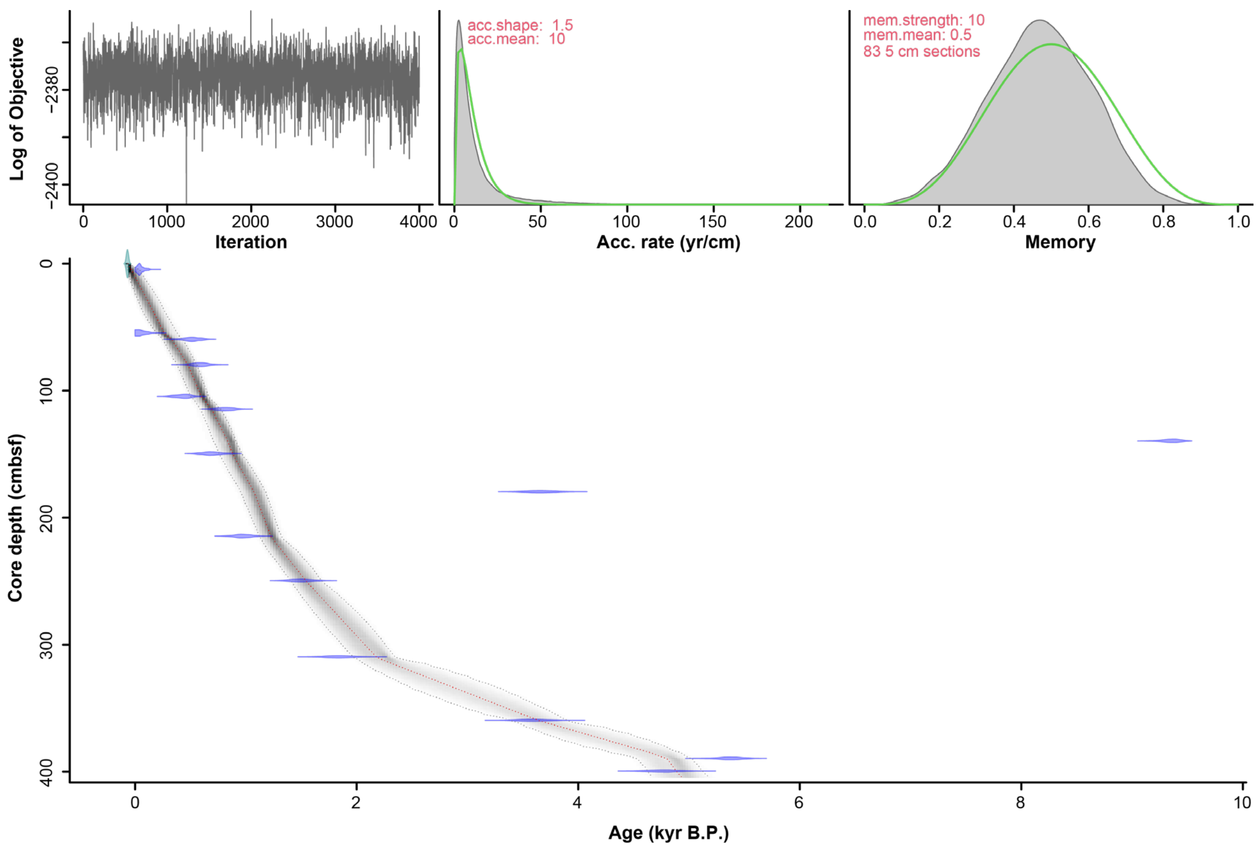

Figure 3. Bayesian age-depth model constructed using Bacon v. 3.2.0 at site HH19-878-GC. Top-left panel displays Markov Chain Monte Carlo iterations (n = 4,000; left), while middle and right panels at the top represent the prior (green) and posterior (gray) distributions for accumulation mean and memory properties, respectively. In the bottom panel, blue symbols indicate the calibrated ^{14}C ages, and the red dotted line illustrates the weighted mean age along with the uncertainty at the 95% confidence level (gray bands).

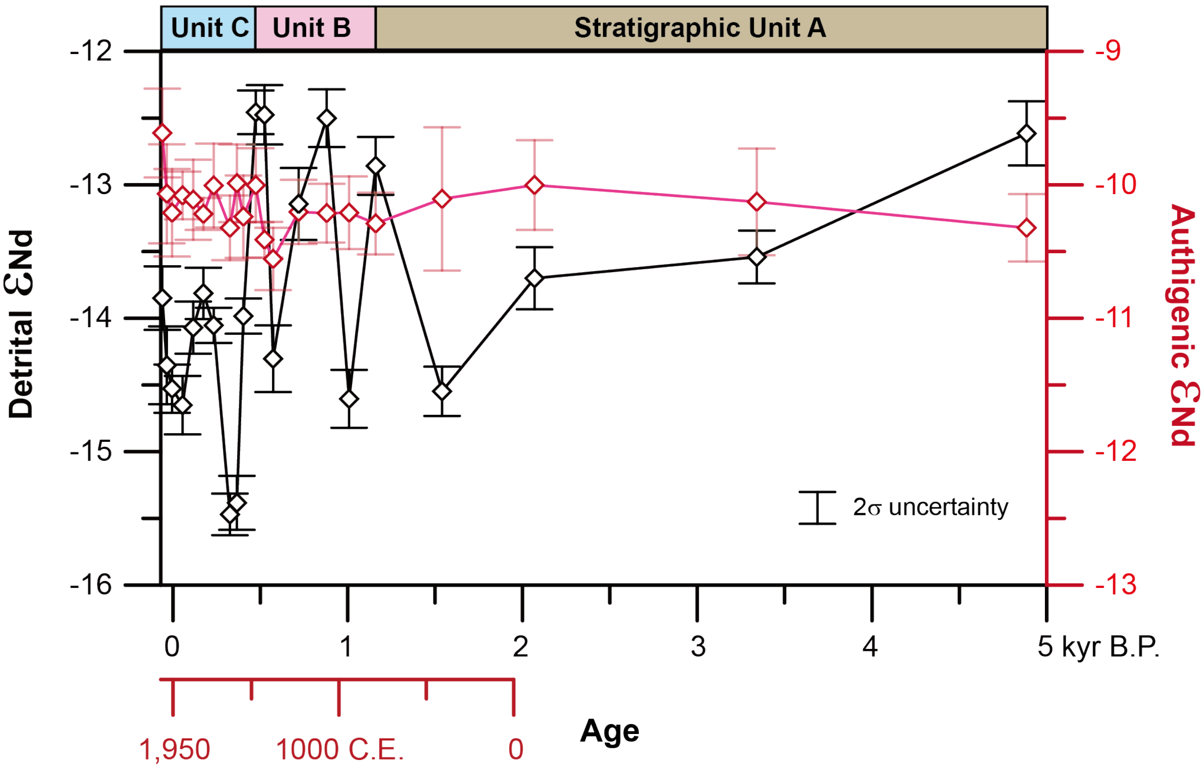

Figure 4. Detrital (black) and authigenic ε_{Nd} records (red) at site HH19-878-GC in Hornsund. Error bars indicate ± 2σ uncertainties.

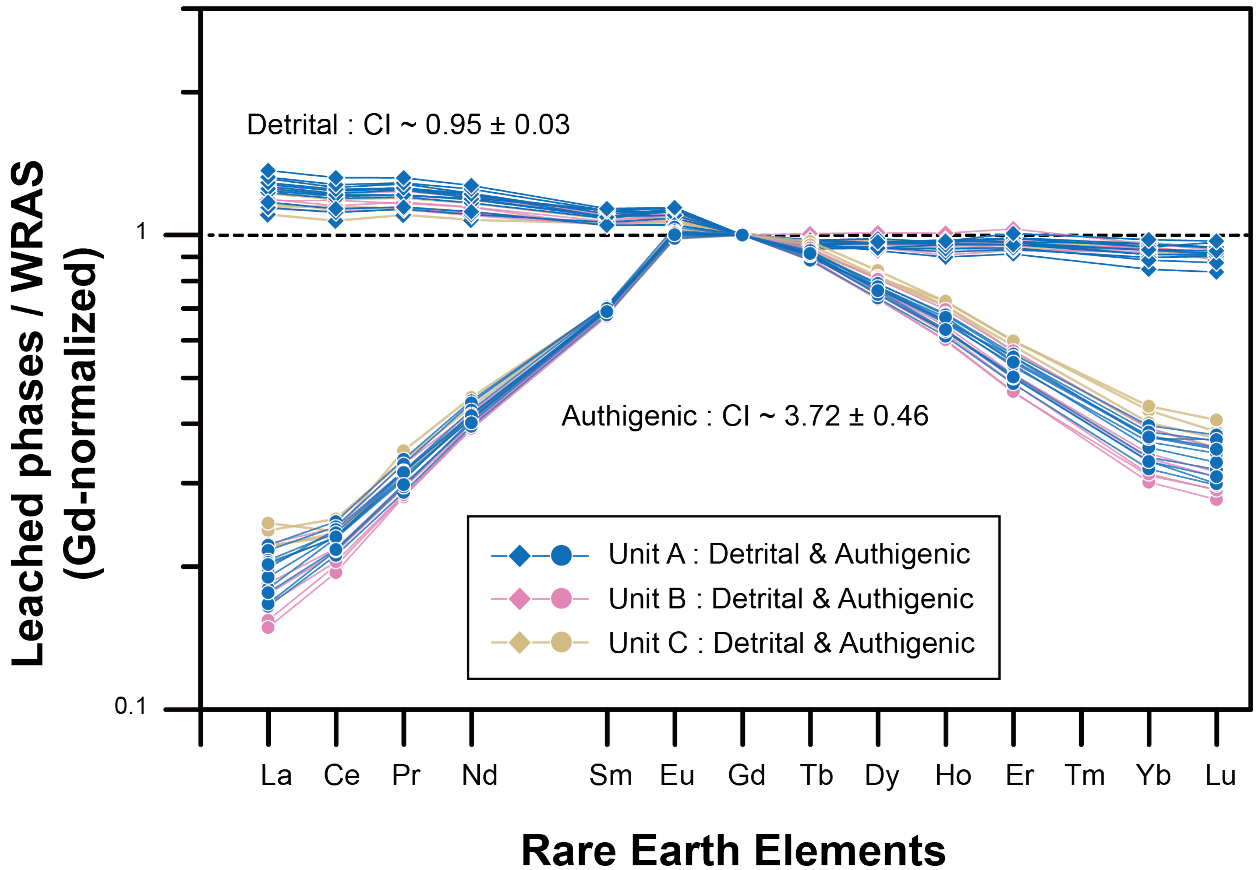

Figure 5. Shale-normalized (WRAS; Bayon et al., 2020) REE patterns for the detrital (diamonds) and authigenic (circles) phases of core HH19-878-GC. While general flat patterns are prevalent in detrital phases (average CI ~ 1), strong mid-REE enrichments are prominent in authigenic phases (average CI ~ 3.7). The degree of mid-REE enrichments in authigenic sediments varies depending on stratigraphic units. Note that the REE data were also normalized by Gd_{WRAS} for clarity.

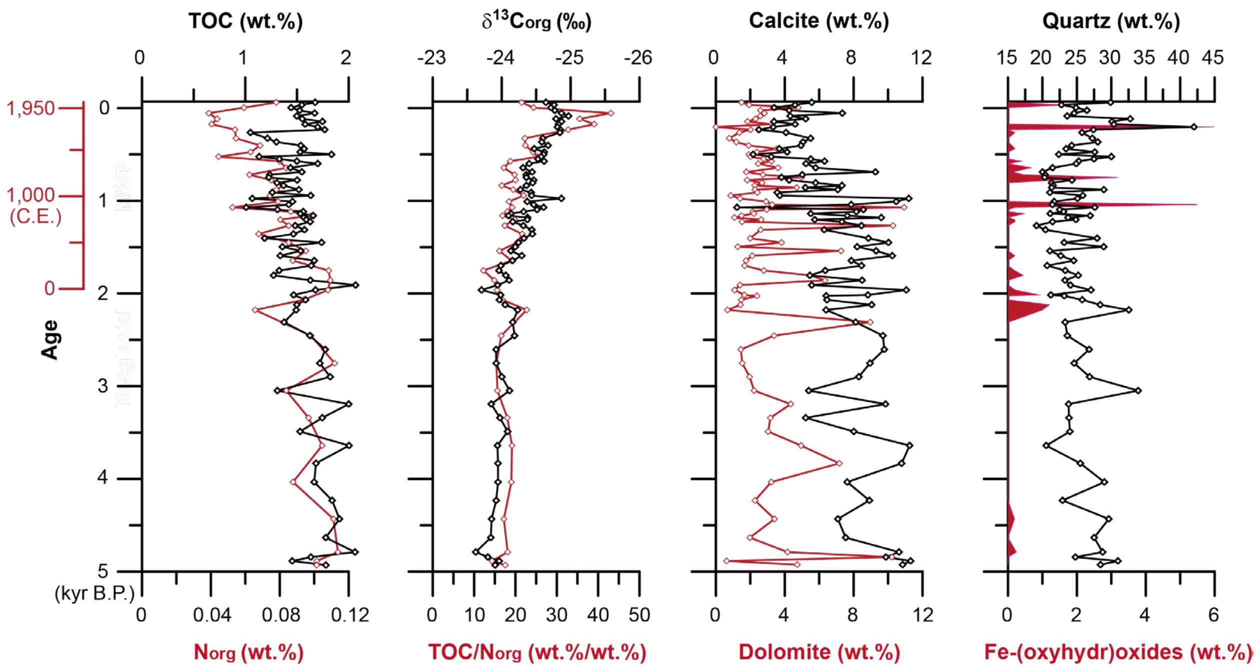

Figure 6. Records of organic chemistry and bulk mineralogy at site HH19-878-GC in Hornsund. The contents of total organic carbon (TOC) and organic nitrogen (N_{org}), $\delta^{13}C_{org}$ values, TOC/N_{org} ratios, the contents of calcite, dolomite, quartz and Fe-(oxyhydr)oxides are shown. Note that the horizontal axis is reversed for $\delta^{13}C_{org}$.

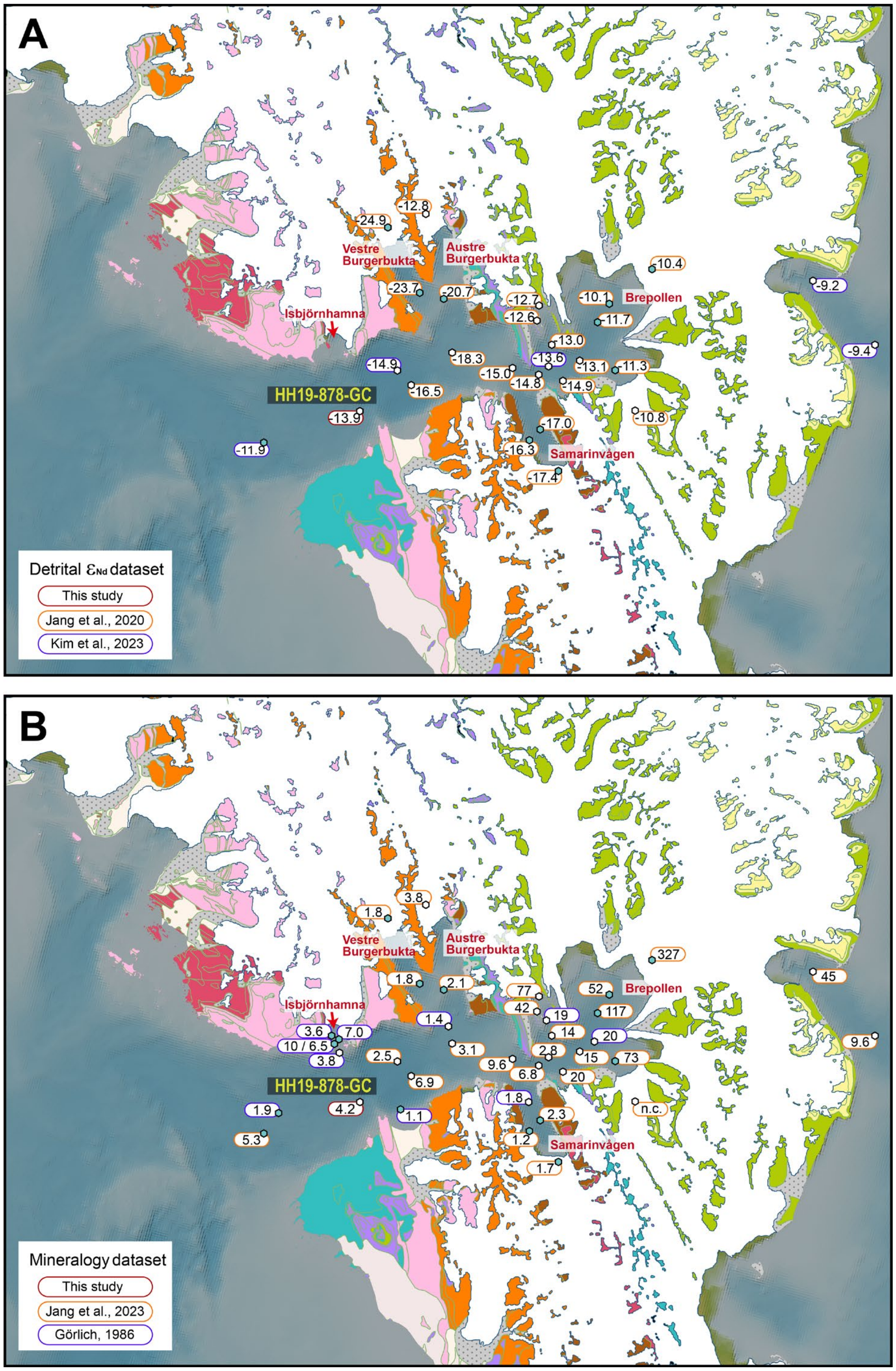

Figure 7. Spatial variability in A) the measured detrital ε_{Nd} values and B) quartz-to-carbonate ratios (wt.%/wt.%) of surface sediments collected from Hornsund. Data marked with blue symbols serve as the representative values for each source, as described in Figure 8.

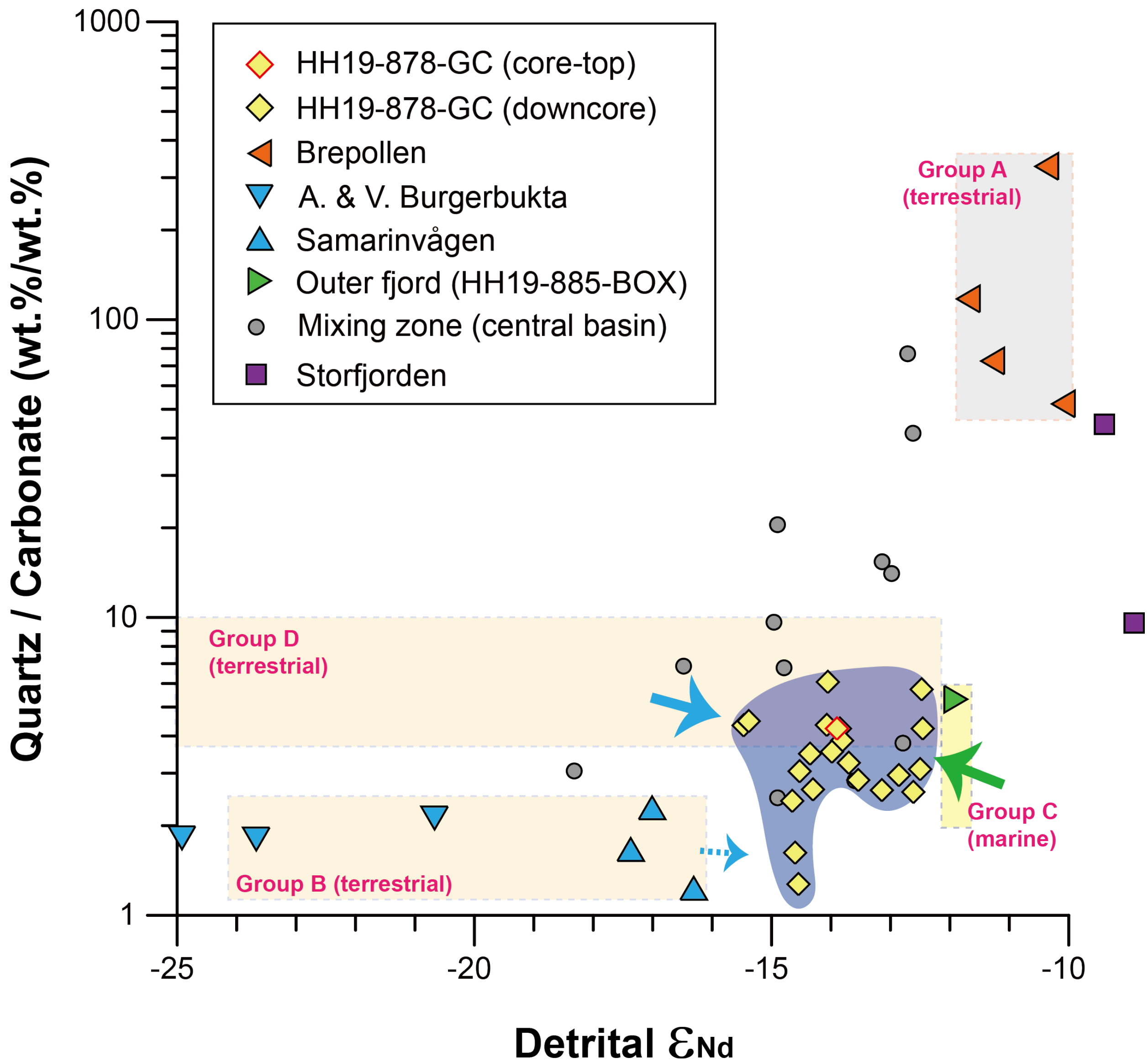

Figure 8. Potential sources for Hornsund sediments and their geochemical (detrital ε_{Nd}) and mineralogical characteristics (quartz-to-carbonate ratios). The plot suggests that sediment deposition at site HH19-878-GC appears to have been influenced by both internal meltwater discharge (blue arrows) and external oceanic inflow (green arrows). Terrestrial inputs likely originate from the Isbjörnhamna regions (Group D), with additional contributions from areas around Burgerbukta and Samarinvågen (Group B).

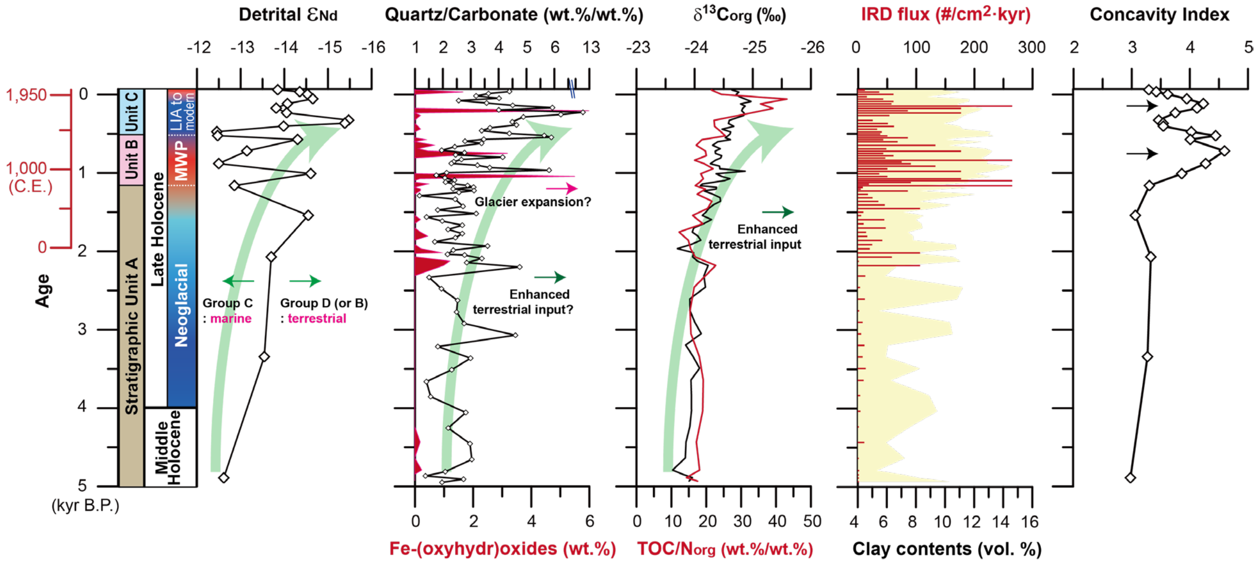

Figure 9. Downcore variability in proxy records at site HH19-878-GC. The records include detrital ε_{Nd}, quartz-to-carbonate ratio, Fe-(oxyhydr)oxide contents, $\delta^{13}C_{org}$ values, TOC/N_{org} ratios, IRD flux (number of grains greater than 1 mm per $cm^2\cdot kyr$), clay contents, and concavity index. Note that the horizontal axis is reversed for detrital ε_{Nd} and $\delta^{13}C_{org}$.